Experimental and theoretical behaviour of large scale loaded steel mesh reinforced concrete ground-supported slabs

Experimental and Theoretical Behaviour of Large Scale Loaded Steel Mesh Reinforced Concrete Ground-Supported Slabs

Joseph P. Rizzuto, Ibrahim G. Shaaban, Spyridon A. Paschalis, Tarek S. Mustafa, Zoubir Benterkia

Abstract

Experimental and theoretical investigations were carried out to study the structural behaviour of loaded steel mesh reinforced concrete ground-supported 6.0 m x 6.0 m by 150 mm slabs. The aim of the study was to benchmark scientific theory with practice. Concentrated loading tests were carried out at the slab centre; at 300 mm, and 150 mm from both the edges and the corners of the slabs. Finite element (FE) numerical modelling results and predicted design values using technical guidance and codes were determined. Nonlinear behaviour under load was captured by the FE modelling. All of the results were evaluated and compared. The experimental tests included the centre and 300 mm edge loading. Other loading positions were evaluated numerically and compared with design guidance. Experimentally for centre loading, failure was predominantly in punching shear at a load of 417 kN. For the 300 mm edge loading, circumferential and radial cracks led to bending and a punching shear failure at a peak value of 369 kN. A notable difference was evident between the experimental and values obtained using the technical guidance. The experimental values were 51.0% higher for the central loading position and 53.2% higher for the 300 mm edge loading position.

Keywords: ground-supported slabs; steel mesh reinforcement; experimental testing; acoustic sensors; acoustic emission measurements; crack patterns; finite element modelling; nonlinear analysis; technical report TR34

Notation:

E_c = the modulus of elasticity for normal strength concrete (NSC) in MPa according to ACI 318M-19 (2019).
f_c` = the ultimate cylinder compressive strength of concrete in MPa.
f = the concrete compressive stress in MPa corresponding to the compressive strain ε.
ε_0 = the concrete compressive strain at the ultimate compressive strength f_c`.
f_r = the modulus of rupture of concrete in MPa according to ACI 318M-19 (2019).
ε_s = reinforcing steel strain at working stresses
ε_y = reinforcing steel strain at yield stress
f_s = reinforcing steel stress at working stage
f_{cr} = stresses of concrete at cracked stage
f_y = yield stress of reinforcing steel
E_s= modulus of elasticity of reinforcing steel
ρ = reinforcement ratio of steel
h = total slab thickness in mm (100 mm < h < 600 mm)
$f_{ctd.fl}$ = characteristic flexural strength of plain concrete
f_{ctm} = characteristic mean axial tensile strength of plain concrete (TR34, 2018, Table 6.1)
γ_m = partial safety factor
a = equivalent radius of contact area of the load
l = radius of relative stiffness (Westergaad, 1926)
E_{cm} = modulus of elasticity of the concrete (N/mm²)
h = slab thickness (mm)
k = modulus of subgrade reaction (N/mm²/mm, taken as N/mm³)

v = Poisson's ratio, taken as 0.2
A_s = the area of steel
f_{yk} = characteristic strength of steel
d=effective depth
$M_n = M_{un}$
$M_p = M_{pfab}$
$k_s = 1 + (200/d)^{0.5} \leq 2.0$
ρ_x, ρ_y = ratio of reinforcement in the x- and y-directions
$\rho_x = A_{sx}/bd$ and $\rho y = A_{sy}/bd$
$\rho_1 = \sqrt{(\rho_x \rho_y)}$
u = length of the perimeter at a distance 2.0 d from the loaded area based on the effective dims of the base plate (TR34, 2018, 7.8.1)

1. Introduction

Reinforced concrete ground-supported slabs transfer the externally applied loads by bearing on the ground. Typical loading which influences load capacity are concentrated loads emanating, for example, from forklift vehicles and racking legs from storage platforms. Theoretical investigations have been carried out to predict the structural response of the slabs-on-grade (Abdel-Rahman et al, 1997; Beckett, 1999, 2003, 2007). A number of experimental tests on ground-supported slabs with various reinforcement regimes under concentrated loading have been carried out (Aboutalebi, 2014; Overli, 2014; Laboudkova, 2016; Xiaochao, 2019). These include slabs of plain concrete, fabric steel mesh, steel and synthetic fibre reinforcement. Loading applied to the slabs was via plates with dimensions of (100 x 100) mm to simulate racking legs and forklifts were included. These tests reported the results under considered different critical loading locations taken at the centre, edges and corners. The majority of these experimental tests were on slabs of smaller dimensions when compared to those typically used in practice.

An experimental test program was presented by Overli (2014) where a slab on ground was subjected to concentrated loading at the centre, edges, and corner positions. Analytical solutions obtained for the ultimate load capacity aligned well with the results obtained in the tests. These also indicated that drying shrinkage caused severe cracking in slabs. The response of the slab was circular cracks formed at the top surface some distance away from the loaded area which agrees with linear elastic theory for slabs on elastic foundations. The failure mode was governed by punching shear for the central load, combined bending and punching shear for the edge loads, and anchoring and punching shear for the corner loads. The capacities were in reasonable agreement with requirements for punching resistance in the design codes (BS EN, 1992-1-1:2004) and traditional yield line solutions for bending failures (Kennedy, G., and Goodchild, C. H., 2004).

Overli's (2014) analytical solutions included Nonlinear Finite Element Analysis (NLFEA). In this NLFEA, the soil was modelled as no-tension bedding and a smeared crack approach employed for the reinforced concrete. Through a parametric study, the finite element model was used to assess the influence of the subgrade stiffness and shrinkage. The numerical analyses, in general, were able to predict first occurrences of cracks. However, by reducing the subgrade stiffness value, a better agreement was achieved between the test and numerical

results. The material characteristics of the subgrade therefore were of importance in this case due to its influence on overall slab resistance.

Aboutalebi et al. (2014) carried out tests on a 6.0 m x 6.0 m x 0.15 m deep plain concrete slab at different critical loading locations, including the centre, edges, and corners. The test results were compared with theoretical values derived using available technical guidelines current at the time which included the 3rd Edition of The Concrete Society, Technical Report 34, Concrete industrial ground floor slabs, (TR34, 3rd Ed, 2003) and the Eurocode (BS EN, 1992-1-1:2004). The authors reported that the theoretical failure loads were significantly lower than the test values.

Sucharda et al. (2018) carried out experimental tests and numerical modelling on a 2.0 m x 1.95 m steel reinforced concrete slab on grade of 120 mm thickness in order to study punching shear failure. It was found that the tested slab failed at a force of 344 kN and an average distance of 1.7 d from the column perimeter, and the shape of the crack was an irregular and oval. The actual value of shear resistance was found to be larger than according to Eurocode (BS EN, 1992-1-1:2004). Additionally, a parametric study of the total load capacity calculation with nonlinear analysis was supplemented by calculations based on existing design Model Code 2010 (*fib*, 2012) and these calculations proved to be useful were found to be time consuming when carrying them out. The numerical model results agreed with the experimental results and the differences between the experiment and numerical modelling results was attributed to the spread and uncertainties in the input concrete and subsoil parameters.

Xiaochao et al. (2019) carried out an experimental study to investigate the potential benefits of embedding geogrids in concrete slabs-on-grade. In addition to four-point bending tests on unreinforced and reinforced concrete beams, large slabs-on-grade were built on top of local soils and aggregate inside a box and tested under monotonic static loading. The results showed that the geogrids carried additional load after cracking was initiated and delayed the collapse failure of the concrete beams. Tests on fully supported slab-on-grade showed that the inclusion of geogrids allowed for the development of secondary cracks after the first cracks which resulted in a greater collapse load.

A parametric study by Abdel-Rahman et al (2017) using NLFEA was performed to utilize the response of slabs-on-grade to loading from vehicles with single wheel axles. The studied parameters were the load position in relation to slab edges, slab proportions, the steel reinforcement content, method of reinforcement arrangement and the modulus of subgrade reaction. The subgrade was represented in the analysis by boundary-spring elements of a non-tension model to simulate the soil-resistance characteristics. The study showed that the load-carrying capacity of slab panels was substantially influenced by panel thickness and to a lesser extent, the modulus of subgrade reaction.

Cajka et al. (2020) carried out experimental, nonlinear finite element three-dimensional computational modelling of a reinforced concrete and fibre reinforced concrete slabs of 2.0 m x 2.0 m and a thickness of 0.15 m interacting with subsoil. The fracture-plastic material of the model was used for concrete and fibre-reinforced concrete. The results showed that the

numerical results obtained by the three-dimensional model were in good agreement with the experimental results.

The above literature shows that the limitations of slabs with a smaller area than those slabs cast in practice, particularly with regard to lifting of corners, were unavoidable in experimental testing.

2. Objectives and Research Significance

This research aims to investigate the structural behaviour and failure modes of a large-scale steel mesh reinforced concrete ground slab-on-grade of the size typically used in practice. Insitu experimental testing recorded behaviour will be compared to the obtained theoretical results. Non-linear finite element analysis (NLFEA) models using ANSYS (ANSYS release 19.2, 2018) are developed to predict the load-displacement curves and failure modes. Design calculations using the latest 4th Edition of The Concrete Society, Technical Report 34, Concrete industrial ground floor slabs, (TR34, 4th Ed, 2018), are validated by comparing the results with the experimental and predicted finite element results. These experimental results will benchmark the reliability of the numerical NLFEA models and the technical guidance output.

3. Experimental Program

An experimental test program was set up for a steel mesh reinforced concrete slab-on-grade subjected to static concentrated loading applied at different critical locations which included the centre and one edge. The slab had a square geometry with dimensions of 6.0 m x 6.0 m and its thickness was 0.15 m which corresponds with the sizes of slabs that are typically cast in practice. The deformations, strains and failure loads of the experimentally tested slab were monitored. A uPVC membrane between the slab and the subbase was placed to minimise moisture transportation and provide a clean surface to cast against. The loading on the slab was via a (100 x 100) mm square plate which was used to represent the loading from typical forklifts and racking legs. See Figure 1 for test and monitoring locations.

3.1 Testing Setup

The experimental testing facilities at the University of Greenwich (UoG), slab mesh details, and cast slab are shown in Figure 2.

3.1.1 Ground conditions

The UoG test rig facility allows for sub-soil excavation, reinstatement and compaction. The test ground conditions were modified, and compressibility of the soil evaluated using a plate equivalent CBR test in accordance with BS 1377: Part 9 (1990). Following twelve CBR tests which were carried out, the average was found to be 12.12 %. The modulus of sub-grade reaction, k modified for plate diameter, CBR tests on the slab area supporting sub-soil gave an average of modulus of sub-grade reaction, k = 0.05 N/mm^3.

3.1.2 Slab loading and monitoring

The loads were applied to the slab via a loading Jack which was attached to a steel top plate attached to a reaction beam. A plywood spreader plate was sandwiched between the (100 x 100) mm steel loading plate and the reinforced concrete slab surface to take up any unevenness in the surface. A (200 x 200) mm steel plate was attached to the steel loading plate upon which were placed four Linear variable differential transducers (LVDTs) numbered 1 to 4. An electronically controlled hydraulic jack applied the loading at a constant rate to the slab. The applied load was recorded from a load pressure cell which was located between the hydraulic jack and the 100 mm square steel loading plate. LVDTs located adjacent to the loading plate and various other positions recorded the slab displacements under loading. The locations of the LVDTs and the loading points varied in each test. Two experimental tests were carried out. The first was located at the internal central location and the second was located at 300 mm from the slab edge. Sampling observation points via LVDT displacement transducers and acoustic sensors were as shown in Figure 1.

The acoustic emissions (AE) testing was performed using Physical Acoustics' Group of R61-AST SN BE07 sensors. The layout of these sensors can be seen in Figure 1 (b) and (c) respectively for tests 1 and 2. Originally conceived as a non-destructive testing technique, the AE sensors during slab testing detected the onset and development of cracking during loading and before the failure load was reached. This was accomplished by directly coupling piezoelectric transducers on the surface of the slab. The rate of loading was incremental and over an average period of 40 minutes for each test. The load increments for the centre loading were: load range 0-100 kN: 25 kN, load range 120-200: 20KN, load range 210-410: 10kN with the failure load at 417 kN. For the 300 mm edge loading: load range 0-100 kN: 25 kN, load range 110-360: 10kN with the peak failure load at 369 kN. The output of each sensor during the applied incremental loading was amplified, filtered and then processed by an 8-channel Physical Acoustics Ltd data logger. The cracking that was detected within the slab was plotted against the corresponding displacement value recorded. Thirty-two plots were recorded of deflection against crack emissions for each test.

3.2 Slab Materials

A total of twelve (150 x 150 x 150) mm concrete cubes were tested with a maximum water/cement ratio of 0.55 The average compressive strength results together with the calculations for tensile strength, the Modulus of Elasticity and the density are shown in Table 1. The strength class of concrete was C32/40 in accordance with Table 6.1 of TR34, 4th Ed (2018). A minimum curing period of 28 days elapsed prior to loading on the slab commencing. The reinforcement was orthogonal steel mesh fabric reinforcement of 6 mm diameter bars at 200 mm centres conforming with Eurocode 2 (BS EN, 1992-1-1:2004+A1 2014) and placed as a bottom layer with a concrete cover of 50 mm.

4. Experimental Results

4.1 Test No. 1 – Centre Loading

The loading position together with the monitoring locations is shown in Figure 3. The slab failed in punching shear and a square depression corresponding to the plate size was visible after the testing. Figure 4 shows the final punching shear failure together with visible crack pattern that developed during loading on the top surface of the slab. The failure load was 417 kN. No circular cracks were visible during the testing. Three typical plots are illustrated in Figure 5 which show the crack propagation profiles as captured by the acoustic sensors at 300 kN and failure at 417 kN. In Figures 6 and 7, the load versus displacement graph caused by

incremental step to failure are presented. As can be seen in Figure 8, the response was approximately linear up to a load level of 400 kN. Figure 9 illustrates the surface deformation profile to the peak failure load of 417 kN.

4.2 Test No. 2 – Edge Loading at 300 mm

Figure 10 shows the loading position together with the locations of the displacement transducers and the acoustic sensors utilised during the 300 mm edge test. For Test No. 2, the (100 x 100 mm) loading and (200 x 200 mm) monitoring plate were centred 300 mm from the slab edge. Figure 11 shows the top surface circumferential and radial cracks from the West and East sides and the vertical cracking on the side of the slab which developed with increasing load. The cracks gradually widened leading to bending and punching shear failure at a failure load level 369 kN. Figures 12 and 13 show the deflections recorded as result of step loading applied at the edge of the slab up to the peak failure load of 369 kN. Figure 14 illustrates the load versus displacement graph caused by incremental step to failure for edge loading. As can be seen from this graph, the slab had a non-linear response from an approximate load value of 150 kN. Figure 15 shows the surface deformation profile achieved under load increments up to 369 kN. These results are discussed further in Section 7.0.

4.3 Crack Patterns

Figure 16 (a) shows a perspective view of half of the slab following the experimental Test 1 at the centre and experimental Test 2 at 300 mm slab edge. A marker pen was used to highlight the visible top surface cracks so that they could clearly be seen and a schematic of the full crack patterns were measured and recorded as illustrated in Figure 16 (b). With increasing loading, new cracks formed closer to the loading areas in accordance with redistribution of forces. The failure mechanisms were punching shear failure at the slab centre and a combination of a bending and punching failure at 300 mm from the slab edge.

This is in agreement with the observations made by Overli (2014) which included when using the same slab to carry out experimental testing; these different locations are sufficiently far enough apart so as not to affect one another.

5. Numerical Modelling of Studied Slabs

ANSYS (ANSYS release 19.2, 2018) was used to numerically model the test slab and loading setup for comparison with the experimental and TR34 (2018) design guidelines output. A correlative study based on the load-displacement relationship and the cracking patterns was conducted. A brief description is included for the finite element modelling of concrete and steel based on the theoretical manual of ANSYS (2018) program.

5.1 Nonlinear Finite Elements Analysis (NLFEA)

A NLFEA was performed to simulate the tested ground bearing slab. The load-displacement curve is an important aspect of verifying the behaviour of ground slabs. The numerical results with the predicted response using the NLFEA were compared with the experimental results to assess their application range and practicality.

5.2 Finite Element Discretization and Solution Technique

5.2.1 Concrete and steel reinforcement

Tables 2 and 3 give the input parameters used in the FE modelling. SOLID65 elements were employed for discretizing the concrete matrix. Both linear and non-linear behaviour of the concrete are considered. SOLID65 is defined by eight nodes. This element is capable of directional integration point cracking in tension and crushing in compression. In this research, tested slabs were typically discretized using an average mesh of size (200 x 200 x 50) mm. The flexural reinforcement of the tested slabs was idealized using the LINK180 element. The axial stress is assumed to be uniform over the entire element and full bond is considered as existing between concrete and reinforcing steel. This element supports uniaxial tension-compression and has the abilities of plasticity, large deflection, rotation, and large strain. The steel plate used for loading the slab was modelled using a SOLID185 element. This element is capable of providing stress distribution over the point of loading area and the supports.

5.2.2 Sub soil

Tables 2 and 3 give the input parameters and structural components which were used in the FE modelling. The soil support was represented by springs using the COMBIN40 element which is a combination of a spring-slider and damper in parallel, coupled to a gap in series. The COMBIN40 element may be used in any analysis.

The element is defined by two nodes, two spring constants K1 and K2 (Force/Length), a damping coefficient C (Force*Time/Length), a mass M (Force*Time^2/Length), a gap size GAP (Length), and a limiting sliding force FSLIDE (Force). (Units listed here apply only to KEYOPT (3) = 0, 1, 2, or 3. If the element is used in an axisymmetric analysis, these values (except GAP) should be on a full 360° basis. A spring constant of 0.0 (for either K1 or K2, but not both) and a damping coefficient of 0.0 will remove these capabilities from the element. The mass, if any, may be applied at node I or node J or it may be equally distributed between the nodes. Thus, a mass can be associated with one or both nodal points. The element has one degree of freedom at each node, either a nodal translation, rotation, pressure, or temperature. The mass, springs, slider, damper, and/or the gap may be removed from the element. The gap size is defined by the fourth element real constant. If positive, a gap of this size exists. If negative, an initial interference of this amount exists. If GAP = 0.0, the gap capability is removed from the element.

The FSLIDE value represents the absolute value of the spring force that must be exceeded before sliding occurs. If FSLIDE is 0.0, the sliding capability of the element is removed, that is, a rigid connection is assumed. If the initial gap is identically zero, the element responds as a spring-damper-slider element having both tension and compression capability. If the gap is not initially zero, the element responds as follows: when the spring force (F1+F2) is negative (compression), the gap remains closed, and the element responds as a spring-damper parallel combination. As the spring force (F1) increases beyond the FSLIDE value, the element slides and the F1 component of the spring force remains constant. If FSLIDE is input with a negative sign, the stiffness drops to zero and the element moves with no resisting F1 spring force. If the spring force becomes positive (tension), the gap opens, and no force is transmitted.

In this study, the spring constant K1 was set to 2000 N/mm while the spring constant K2, the GAP, the mass, and the force FSLIDE were set to 0.0.

5.2.3 Analysis considerations

For the linear stage, the concrete is assumed to be an isotropic material up to cracking. For the non-linear segment, the concrete may undergo plasticity. Using the Newton-Raphson method, the numerical solution scheme adopted for non-linear analysis is an incremental load procedure based on the iterative solution. The used convergence criterion is based on the iterative nodal displacement where only transitional degrees of freedom were considered.

5.3 Constitutive Modeling for Concrete

The assigned concrete material model in this study (SOLID65 element) is characterized by its capability to predict the failure of brittle materials. Both cracking and crushing failure modes are included. The considered idealized curve of the uniaxial stress-strain relationship of the concrete in this study is illustrated in Figure 17 (a). In tension, the stress-strain curve for concrete is assumed to be linearly elastic up to the ultimate tensile stress. To compute the multilinear isotropic stress-strain curve for the concrete, the following equations were used

$$E_c = 4700\sqrt{f_c`} \quad (1)$$

$$f = \frac{E_c \varepsilon}{1 + \left(\frac{\varepsilon}{\varepsilon_0}\right)^2} \quad (2)$$

$$\varepsilon_0 = \frac{2f'_c}{E_c} \quad (3)$$

$$E_c = \frac{f}{\varepsilon} \quad (4)$$

$$f_r = 0.623\sqrt{f_c`} \quad (5)$$

All parameters related to the concrete modelling are reported in Table (2). The parameters in the computing model are consistent with the experimental parameters. Poisson's ratio for concrete (υ_c) is considered as 0.2. The shear transfer coefficients for a closed crack (β_c) and an open crack (β_t) are assumed to be 0.8 and 0.2, respectively. To overcome the problem of stress locking and mesh sensitivity, the rational crack model was considered in which the crack is always oriented perpendicular to the principal tensile stress. Cracking and crushing locations of concrete elements are assumed to be at integration points. The confinement effect is not considered in the computing model. The subsoil was represented by linear elastic model with the parameters reported in Table (2).

5.4 Constitutive Modeling for Steel

The average stress-strain curve developed by Soroushian and Lee (1989) for steel bars embedded in concrete is used in this study as illustrated in Figure 17 (b). The stress-strain relationship is expressed by two straight lines as follows:

For $\varepsilon_s \leq \varepsilon_n$:

$$f_s = E_s \varepsilon_s \quad (6)$$

and for $\varepsilon_s \geq \varepsilon_n$:

$$f_s = f_y\left[(0.91-2B)+\left(0.02+0.25B\frac{\varepsilon_s}{\varepsilon_y}\right)\right] \quad (7)$$

Where $\varepsilon_n = \varepsilon_y(0.93-2B)$.

And the parameter B is given as $\left(f_{cr}/f_y\right)^{1.5}/\rho$

The recommended value of f_{cr} is given as:

$$f_{cr} = 0.31\sqrt{f_c'} \quad \text{in MPa} \quad (8)$$

5.6 Finite Element Models of the Tested Slabs

The area and spacing of bar elements were identical to the experimental specimens. The concentrated load was also applied to the top surface of slabs as a central (internal) loading, edge loading and corner loading. The initial Young's modulus in concrete has been considered as 33 kN/mm^2; and the steel modulus as 200 kN/mm^2. Figures 18 and 19 show typical numerical idealization of the reinforced concrete and supporting soil, and the concrete with embedded steel reinforcement mesh elements respectively.

A summary of the FEA results for the slab tests 1 at the centre and 2 at 300 mm from the edge are given in Table 4 and discussed in Section 7.0.

5.7 Load Displacement Curves and Crack Patterns

Figures 20 shows comparisons between experimental and FEA numerically predicted load-displacement curves for centre and at 300 mm edge loading. It can be seen that the numerical modelling predicted results are in good agreement with the recorded experimental results. Figure 5 shows the acoustic sensors recorded crack development for load increments to failure for the slab at centre loading. Comparing these with the FEA crack propagation profiles shown in Figure 21, it can be seen that there is a good agreement between numerical prediction and experimental observation. Figures 22, 23, 24 and 25 illustrate the predicted crack patterns on the slab top surface and soffit for each loading position.

5.8 FEA Edge and Corner Loading Locations

The FEA predicted theoretical load-displacement relationships for the 300 mm and 150 mm corner loading positions and the 150 mm edge are shown in Figure 20. It can be seen that for the 300 mm corner loading, the maximum displacement was 13 mm at a failure load of 220 kN. For the 150 mm corner loading, the maximum displacement was 10.4 mm at a failure load of 206 kN. For the 150 mm edge loading, the maximum displacement was 13.4 mm at a failure load of 326 kN.

6. Predicted Behaviour according to TR34, 4th Ed, (2018)

Design guidance is in keeping with good practice, updated from time to time. The last update to TR34 was published in 2018 as the 4th edition which included guidance on how to take

account of the soil contribution response to slab loading. Other editions of TR34 include the 3rd Ed., (2003), the 2nd Ed., (1994) and the 1st Ed., (1988).

6.1 Theoretical Calculations

6.1.1 Bending

TR34, 4th Ed., (2018) recommends that the characteristic flexural strength of plain concrete, $f_{ctd.fl}$ should be taken based on Eurocode 2 (BS EN, 1992-1-1:2004+A1 2014) from section 6.1.1, for slabs thinner than 600 mm, where:

$$f_{ctd.fl} = f_{ctm} [1.6 - (h/1000)/\gamma_m] \quad \text{Eqn. 1 (TR34, 2018)}$$

Theoretical calculations for the steel fabric reinforced slab loading locations were undertaken in accordance with Chapters 6 and 7 of TR34. 4th Ed (2018), using the Meyerhof Equations 9 to 14 for bending (Meyerhof, 1962) (See 7.8.3 design equations for a single point load, TR34. 4th Ed (2018).

(i) For an internal load with:

$a/l = 0$: $P_{u,0} = 2\pi (M_p + M_n)$ (9)

$a/l \geq 0.2$: $P_{u,0.2} = 4\pi (M_p + M_n)/[1 - a/3l]$ (10)

(ii) For a free edge load with:

$a/l = 0$: $P_{u,0} = [\pi (M_p + M_n)/2] + 2 M_n$ (11)

$a/l \geq 0.2$: $P_{u,0.2} = [\pi (M_p + M_n) + 4 M_n]/[1 - 2a/3l]$ (12)

(iii) For a free corner load with:

$a/l = 0$: $P_{u,0} = 2 M_n$ (13)

$a/l \geq 0.2$: $P_{u,0.2} = 4.0 M_n / [1 - (a/l)]$ (14)

Where:

The moment capacity of plain concrete,

$M_{un} = f_{ctd,fl} (h^2 / 6)$ Eqn. 2, TR34, 4th Ed, 2018, 6.3.1

The moment capacity, $M_{p,fab}$

$M_{p,fab} = 0.95 A_s f_{yk}/\gamma_m d$ Eqn. 3, TR34, 4th Ed, 2018, 6.3.2

$M_n = M_{un}$

$M_p = M_{pfab}$

M_n = negative (hogging) resistance moment of the slab (kNm), taken to be that of plain unreinforced concrete

M_p = ultimate positive (sagging) resistance moment of the slab (kNm), taken to be that of the reinforced concrete

Figures 26 and 27 provide a schematic of the distribution of elastic bending moments and the development of radial and circumferential cracks in concrete ground-supported slabs. Figure 28 provides the definitions of loading conditions.

6.1.2 Shear

The Shear capacity of a slab according to TR34 (2018) should be checked at:

(i) The face of the contact face
(ii) The critical perimeter at (2.0 d) from the face of the contact area

Figure 29 illustrates the critical perimeters for punching shear for internal, edge and corner loading.

6.1.2.1 Shear at the Face of the Support

In accordance with Eurocode 2 (BS EN, 1992-1-1:2004+A1 2014), irrespective of the amount of any reinforcement in the slab, the shear stress at the face of the contact area should not exceed a value, v_{max} given by:

$$v_{max} = 0.5\, k_2\, f_{cd} \qquad (15)$$

Where:

f_{cd} = *design concrete cylinder compressive strength* = $f_{ck} / \gamma c$
k_2 = $0.6\,(1 - f_{ck} / 250)$ [k_2 = 'v_1' in Eurocode 2]
f_{ck} = *characteristic concrete cylinder compressive strength*

Hence, maximum load capacity in punching, $P_{p,max}$, is given by:

$$P_{p,max} = V_{max}\, u_o\, d \qquad (16)$$

Where:

u_o = *length of the perimeter at the face of the load area based on the effective dimensions of the base plate (*TR34, 2018, 7.8.1*).*

6.1.2.2 Shear on the critical perimeter

The Shear on the critical perimeter can be defined for unreinforced concrete and reinforced concrete containing fabric or steel bar reinforcement

(i) For unreinforced concrete:

The min shear strength, $v_{Rd,c,min} = 0.035\, k_s^{1.5}\, f_{ck}^{0.5}$ (17)

Where:

$k_s = 1 + (200/d)^{0.5}$ [k_s = 'k' in Eurocode 2)]
d = effective depth

$k_s \leq 2.0$ [6.2.2, Eurocode 2)]

Shear stress is checked on the critical shear perimeter at 2.0 d from the face of the contact area.

(ii) For reinforced concrete containing fabric or steel bar reinforcement:

The average shear stress that can be carried by the concrete on the shear perimeter, $v_{Rd,c}$

$$v_{Rd,c} = 0.18\, k_s / gc\, (100\, \rho_1\, f_{ck})^{0.33} \geq 0.035\, k_s^{1.5}\, f_{ck}^{0.5} \qquad (18)$$

Where:

$k_s = 1 + (200/d)^{0.5} \leq 2.0$
$\rho_1 = \sqrt{(\rho_x\, \rho_y)}$
ρ_x, ρ_y = ratio of reinforcement in the x- and y-directions
$\rho_x = A_{sx}/bd$ and $\rho_y = A_{sy}/bd$

Thus, the slab load capacity, P_p

$$P_p = v_{Rd,c}\, u_1\, d \qquad (19)$$

Where

*u_1 = length of the perimeter at a distance 2.0 d from the loaded area based on the effective dims of the base plate (*TR34, 2018, 7.8.1*).* See Figure 29 for critical perimeters.

Figure 30 shows the FEA and experimental critical perimeters for punching shear for internal, edge and corner loading considered for tests 1 to 5. Figure 31 illustrates the minimum perimeter lengths for loading positions loading 2 and 3 with loading conditions 4 and 5 similar. Figure 32 shows the simplified 'inverted cone' ground pressure distribution within the critical perimeter for an internal load and an edge load given in TR34, 4th Ed, Appendix F.

7. Discussion of Results

The summary of the experimental, theoretical and numerical results is presented in Table 5. When comparing the experimental and FEA load displacement curves for the Centre loading shown in Figure 20, it can be seen that the FEA predicts an overestimate of the slab load capacity at displacements of 2 mm by 26.7%; at 4 mm by 6.8% and at 5 mm by 4.5%. The experimental failure load was measured at 417 kN and a peak displacement of 5.7 mm. The FEA failure load was predicted as 422 kN at peak displacement of 5.2 mm. From Table 4 (a) and Table 4 (b) comparison of load values at first crack show that the experimental load was measured at 40 kN at a displacement of 0.9 mm; the FEA predicted load value was 134 kN at a displacement of 1.45 mm.

Figure 20 illustrates the experimental (Exp) and FEA (Num) load verses displacement curves for (i) the Centre and 300 mm Edge loadings, and (ii) the FEA predicted curves for 150 mm Edge, 300 mm Corner and 150 mm Corner loading.

The experimentally recorded values of failure load verses displacement for the Centre loading was 417 kN at 5.7 mm respectively and the observed behaviour was linear in nature. The FEA predicted failure load verses displacement for comparison was 422 kN at 5.2 mm. The FEA predicted failure load was overestimated by 1.2% and displacement was underestimated by 8.7%. The FEA predicted failure load is therefore in good agreement with the experimental values.

For the 300 mm edge loading, the experimentally recorded behaviour was non-linear in nature with a peak load value recorded prior to the failure load being reached. A peak value of 369 kN was experimentally observed which occurred at a displacement of 17.0 mm. The failure load verses displacement values were 355 kN at 19.0 mm respectively. The FEA predicted failure load verses displacement was also non-linear in nature. For comparison, the failure load verses displacement values were 353 kN at 16.0 mm. The FEA model 300 mm Edge loading was in good agreement with the failure load but predicted this would occur at a lower displacement value than that recorded experimentally. The FEA predicted failure load was underestimated by 0.6% and displacement was underestimated by 15.8%. This displacement discrepancy was due to the FEA not predicting a localised peak load prior to failure being reached and will need to be considered further in future FEA modelling.

The 150 mm edge loading displayed similar non-linear behaviour characteristics to the 300 mm edge loading. The FEA predicted failure load verses displacement was 360 kN at 19.2 mm respectively. The FEA predicted failure load verses displacement for the 150 mm and 300 mm corner loading shown in Figure 20 can be seen to display similar non-linear behaviour characteristics to each other. The predicted failure loads were 220 kN at 13.0 mm displacement for the 150 mm corner loading and 249 kN at 15.6 mm displacement for the 300 mm corner loading.

When comparing the experimental and FEA load displacement curves for the 300 mm edge loading shown in Figure 20 it can be seen that the FEA predicts an overestimate of the slab load capacity at displacements of 6 mm by 12.0%; and at 15 mm underestimated by 3.3%. The experimental failure load was measured at 369 kN at a peak displacement of 20.5 mm. The FEA failure load was predicted as 353 kN at peak displacement of 16.0 mm. Table 4 (a) and Table 4 (b) comparison of load values at first crack show that the experimental load was measured at 177 kN at a displacement of 4.0 mm; the FEA predicted load value was 115 kN at a displacement of 2.3 mm.

The failure loads from the experimental testing and the FEA predicted when compared to the TR34 design values show that there is a factor of safety of 2.04 and 2.07 respectively.

Comparing the FEA with TR34 predicted shear at (2d) from the loaded face, for T1, the factor of safety (FOS) is 2.5; for T2, FOS is 2.1; for T3, FOS is 2.7; for T4 at 300 mm from the corner, FOS is 1.5; for T5 at 150 mm from the corner, FOS is 2.3. Comparing the FEA with TR34 predicted bending, for T1, the factor of safety (FOS) is 2.09; for T2, FOS is 2.21; for T3, FOS is 3.25; for T4 at 300 mm from the corner, FOS is 2.04; for T5 at 150 mm from the corner, FOS is 2.99. Thus, T4 shear resistance at (2d) from the loaded area has the lowest FOS at 1.5. Currently, EC2 (BS EN, 1992-1-1:2004+A1 2014) guidance on critical control perimeters around loaded area close to slab openings as illustrated in Figure 31 should be considered.

Table 5 depicts the design guidance theoretical values for bending using the Meyerhof's equations (Meyerhof, 1962) together with the punching shear values in comparison with the test results and the values obtained from the finite element analysis.

It can be noticed from the experimental results that for the load centred at 300 mm from the slab edge, the failure load is 88.5 % of the maximum internal load. From the results of Table 5, very good agreement can be observed between the experimental results and the numerical results for both the internal and the edge loading. The theoretical values obtained using TR34, 4th Ed (2018) were significantly lower than the experimental results. More specifically, for internal loading, a maximum load value of 422 kN was recorded from the numerical investigation and a value of 417 kN was recorded from the experimental investigation. The TR34, 4th Ed (2018) theoretical value obtained was calculated at 204 kN which is 48% of the value obtained numerically and 49% of the value obtained experimentally.

Very good agreement was also noticed between the experimental and the numerical results for edge loading. In this case, a maximum numerical FEA predicted value of 353 kN was obtained which is close to the experimental value of 369 kN.

When comparing the numerical and theoretical values at distance (2d) from the face of the loaded area, consistently lower values were obtained from the theoretical model. In this case,

the maximum load obtained from the theoretical model in different positions was in the range of 37 % to 66% of the maximum load obtained from the numerical model.

The FEA predicted surface cracks and failure shown in Figure 21 (a) and (b) for the central loading clearly illustrate very uniform and symmetrical patterns. The top surface central pattern is in very good agreed with the acoustic emissions crack patterns shown in Figure 5 (c). For the 300 mm Edge loading, Figure 16 (a) and (b) show the extent of the visible crack patterns which radiate concentrically from the load position and these can be compared with the FEA predicted patterns shown in Figure 22 (b). The experimentally recorded visible surface cracks shown in Figure 16 when compared to the FEA predicted surface patterns shown in Figures 21 and 22 illustrate that crack thicknesses are important to extract in order that they can be categorised into main and secondary cracking modes.

The results of the present study are in agreement with previous studies in the field. Aboutalebi *et al*. (2014) studied the structural behaviour of plain concrete ground supported slabs loaded in different critical loading locations such as the center, edges and corners. The dimension of the slab in this study was identical to the dimensions of the slab of the present investigation. However, the concrete strength in the present investigation was slightly less than that of Aboutalebi *et al*. (2014). That's why Aboutalebi *et al*. (2014) found that the load at 300 mm from the edge was 92% of the maximum internal load while the load at the edge was 88.5% of the internal load in the present investigation. An interesting finding of this study, which is in agreement with the existing study, is that the theoretical values derived from available design codes at the time (TR34, 3rd ed. 2003) were significant lower compared to the test values. This indicates that further investigation on the reliability of existing technical guidelines is required.

Overli (2014) studied the behaviour of ground supported Reinforced Concrete slab subjected to concentrated loading at the center, at the edges and at the corners. The dimensions of his study were 3.50 m x 3.50 m x 0.12 m deep slab which almost half those of the present study. In addition, Overli (2014) added a layer of 100 mm of insulation used to represent the supporting soil. The failure mode of the slab in this study was similar with the failure mode of the present study. The critical perimeters for punching shear failure for internal and edge loading applied to the ground slabs in the present study are shown in Figure 30. For loading at the center, the slab failed in punching shear and cracks were observed on the top surface of the slab as shown in Figure 16. The failure mode for loading at the edge was governed by bending and punching and circular cracks formed the top surface. In this study however the loads at the two edges were 39% and 36% of the internal loading. These values are lower compared to the values obtained in the existing study and also reported by Aboutalebi *et al* (2014).

8. Conclusions

The present research focused on the structural behaviour of loaded steel mesh reinforced concrete ground supported slabs. Full Scale experimental tests were carried out at different critical loading locations which included the centre, edges and corners of a ground supported slab of dimensions 6.0 m x 6.0 m x 0.15 m thickness. Finite element modelling was developed to verify the experimental results. The design guidelines in 4th Edition of TR34 were verified versus experimental and numerical results. The following conclusions can be drawn from the results:

For the central loading, the slab failed in punching shear and a characteristic indentation under the test plate was visible after the testing. The failure load was 417 kN and cracks were visible on the top surface of the slab.

For the 300 mm distance edge loading, vertical cracks on the side of the slab appeared and with increasing load gradually widened followed by circumferential and radial cracks leading to punching failure at 369 kN. With increasing loading, new cracks formed closer to the loading area. This is in accordance with redistribution of forces closer to the loaded area as the slab starts to crack.

The acoustic emissions (AE) testing was performed using Physical Acoustics' Group of R61-AST SN BE07 type sensors. Originally conceived as a non-destructive testing technique, the AE sensors during slab testing detected the onset and development of cracking during loading and before the failure load was reached. This was accomplished by directly coupling piezoelectric transducers on the surface of the slab. The rate of loading was incremental and over a period of 40 minutes for each test. The cracking that was detected within the slab was plotted against the corresponding displacement value recorded. 32 plots were recorded of deflection against crack emissions for each test.

Finite element predictions of crack propagation profiles at the slab centre and at the edges in load increments to failure were in good agreement with experimental observations. Comparisons between experimental and numerically predicted load-displacement curves at edge 300 mm and at centre showed good agreement.

Based on this good agreement, the FEA predicted theoretical load displacement relations and crack pattern for corner loading at 300 mm and 150 mm and edge loading at 150 mm were for the 300 mm corner loading, the failure load was 220 kN; for the 150 mm corner loading, the failure load was 206 kN; and for the 150 mm edge loading, the failure load was 326 kN.

A notable difference was noticed between the test results and values calculated by the equations in technical guidance reports. Theoretical values obtained using TR34, 4th Ed (2018) were significantly lower than the experimental results and finite element results by 51% and 52%, respectively. Therefore, significant reserve capacity is apparent in slabs designed using the technical guidelines.

The results of the present study further demonstrate the significance of carrying out full scale tests on slab sizes similar to those used in practice.

References

Abdel-Rahman, G. T. (1997). 'Non-Linear Finite Element Analysis of Reinforced Concrete' CERM, Al-Azhar University, V. 19, No. 4, pp. 543-560.

Abdel-Rahman, G.T., El-Ghaly, A.E., and Shaaban, I. G., (2017), A parametric study of reinforced concrete slabs-on-grade in industrial buildings International research journal of engineering and technology (irjet) e-issn: 2395-0056 volume: 04 issue: 09

Aboutalebi, M., Alani, A. M., Rizzuto, J.P. and Beckett, D. (2014) Structural behaviour and deformation patterns in loaded plain concrete ground supported slabs. Journal of Structural Concrete. Ernst & Sohn. 15 (1), pp 81 - 93. ISSN: 1464 4177.

ACI Committee 318, (2019), 'Building Code Requirements for Structural Concrete and Commentary, Metric, ACI 318M-19, ACI 'American Concrete Institute', 38800 Country Club Drive Farmington Hills, MI 48331 U.S.A.

ANSYS–Release Version 19.2, (2018) 'A Finite Element Computer Software and User Manual for Nonlinear Structural Analysis', ANSYS Inc. Europe, Canonsburg, PA 15317 Ltd. http://www.ansys.com

Beckett D., (1999) A comparison of thickness design methods for concrete industrial ground floors, Teknische Akademie Esslingen, 4th International Colloquium January 12-14, Industrial Floors 99, Vol. 2, page 159.

Beckett D., (2003) Strength and serviceability design of concrete industrial ground floors, Teknische Akadamie Esslingen, 5th International Colloquium January 21-23, Industrial Floors 03, Vol. 2, page 601.

Beckett D., (2007) Concrete ground slab test facilities at the University of Greenwich: an update, Teknische Akademie Esslingen, 6th International Colloquium January 16-18, Industrial Floors 07, Vol. 2, page 707.

British Standards Institution, BS EN 1992-1-1: 2004 (incorporating corrigendum 2014), Eurocode 2: Design of concrete structures Part 1-1: General rules and rules for buildings.

British Standards Institution, BS 1377: Part 9: 1990, Methods for test for soils for civil engineering purposes. In-situ tests, Replaced By: BS EN 1997-2:2007, BS EN ISO 22476-2:2005+A1:2011, BS EN ISO 22476-3:2005+A1:2011, BS EN ISO 22476-1:2012.

Cajka, R, Marcalikova, Z, Bilek, V, and Sucharda, O, (2020), 'Numerical Modelling and Analysis of Concrete Slabs in Interaction with Subsoil', Sustainability MDPI, Vol. 12, No. 9868; Doi: 10.3390/su12239868, www.mdpi.com/journal/sustainability

fib (2012) Model code 2010 – Final version – Volumes 1 and 2.. Fédération Internationale du Béton (fib), Lausanne, Switzerland.

Kennedy, G., and Goodchild, C. H., (2004), 'Practical Yield Line Design An introduction to the practical use of Yield Line Theory in the design of economic reinforced concrete slabs, including examples of design of flat slabs, raft foundations and refurbishment', TCC/03/3, ISBN 1-904818-08-0.

Labudkova, Jana and Cajka Radim. (2016) Experimental measurements of subsoil—structure interaction and 3D numerical models. Perspectives in Science (2016) **7**, 240—246.

Meyerhof G.G.W., (1962) Load carrying capacity of concrete pavements. Journal of the Soil Mechanics & Foundations Division. Proceedings of the American Society of Civil Engineers (ASCE), Vol. 88, June, pp. 89-166.

Model Code 2010 (2012), Final Draft, Fib, Bulletin No. 65 and 66, 1-2.

Overli, Jan (2014), Experimental and Numerical Investigation of Slabs on Ground Subjected to Concentrated Loads. Central European Journal of Engineering. Cent. Eur. J. Eng. • 4(3) • 2014 • 210-225, DOI: 10.2478/s13531-013-0159-9.

Soroushian, P., and C. Lee. (1989), Constitutive modelling of steel fibre reinforced concrete under direct tension and compression, Cardiff, University of Wales, pp363–377.

Sucharda, O., Smirakova, M., Vaskova, J., Mateckova, P., Kubosek, J., and Cajka, R., (2018), 'Punching Shear Failure of Concrete Ground Supported Slab', International Journal of Concrete Structures and Materials, DOI 10.1186/s40069-018-0263-6

The Concrete Society, Technical Report 34, Concrete industrial ground floor slabs – a guide to their design and construction, 1st edition, 1988.

The Concrete Society, Technical Report 34, Concrete industrial ground floor slabs – a guide to their design and construction, 2nd edition, 1994.

The Concrete Society, Technical Report 34, Concrete industrial ground floor slabs – a guide to their design and construction, 3rd edition, 2003.

The Concrete Society, Technical Report 34, Concrete industrial ground floor slabs – a guide to design and construction, 4th edition, Jan. 2018.

Westergaard H.M., (1926) Stresses in concrete pavements computed by theoretical analysis. Public Roads Vol. 7, No. 2.

Xiaochao Tang, Mohamad N. Jlilati, and Isaac Higgins; (2019) Concrete Slab-on-Grade Reinforced by Geogrids, Eighth International Conference on Case Histories in Geotechnical Engineering, Geo-Congress.

Table 1: The compressive strength test results

150x150x150mm Cubes tested	Days			
	7	14	28	48
Characteristic compressive cube Strength, $f_{cu,}$ (average), N/mm² (MPa)	25.12	33.31	39.05	40.23
Average Density, (Kg/m³)	2328.8	2324.9	2326.9	2317.5
EC2 (BS EN, 1992-1-1:2004+A1 2014), Table 3.1, Characteristic compressive cylinder strength, f_{ck} (equivalent averaged measured), N/mm² (MPa)	20.0	27.0	31.0	32.0
$f_{ctm\ (0.05)}$, N/mm² (MPa)	1.50	2.27	2.44	2.49
E_{cm}, kN/mm² (GPA)	30.0	32.04	33.09	33.35

Table (2): Input parameters for concrete and reinforcement in finite element modelling

Material Type	Parameter	Definition	Value
Concrete (SOLID65)	$f_c^{'}$	The ultimate cylinder compressive strength of concrete in MPa	32.0
	f_r	The modulus of rupture of concrete in MPa	3.52
	f_{cr}	Stresses of concrete at cracked stage in MPa	1.75
	E_c	Modulus of elasticity for concrete in GPa	33.0
	ε_o	The concrete compressive strain at the ultimate compressive strength f_c`	0.0019
	υ_c	Poisson′s ratio	0.2
	β_c	The shear transfer coefficient for a closed crack	0.8
	β_r	The shear transfer coefficient for an open crack	0.2
Reinforcement (LINK180)	f_y	Yield stress of reinforcing steel in MPa	500
	E_s	Modulus of elasticity for reinforcing steel in GPa	200
	υ	Poisson′s ratio	0.3
Steel Plates (SOLID185)	E_s	Modulus of elasticity for reinforcing steel in GPa	200
	υ_s	Poisson′s ratio	0.3
Soil (COMBIN40)	*K1*	First spring constant in N/mm	2000
	K2	Second spring constant in N/mm	0.0
	Fslide	Sliding force in N	0.0
	GAP	Gap size in mm	0.0
	EMIS	Emissivity of soil	0.78

Table (3): Finite Element Representation of Structural Components

Structural Component	Element Designation in ANSYS	Element Description
Concrete	SOLID65	This element is defined by eight nodes and capable of directional integration point cracking in tension and crushing in compression
Reinforcement	LINK180	This element supports uniaxial tension-compression and has the abilities of plasticity, large deflection, rotation, and large strain
Steel Plate	SOLID185	This element is capable of providing stress distribution over the point of loading area and the supports
Subsoil	COMBIN40	This element is defined by two nodes, two spring constants K1 and K2 (Force/Length), a damping coefficient C (Force*Time/Length), a mass M (Force*Time2/Length), a gap size GAP (Length), and a limiting sliding force FSLIDE (Force)

Table 4 (a): Summary of experimental results for slab tests 1 and 2

Test No	Slab location	Load at 1st crack, (kN)	Load at failure, (kN)	Average displacement (mm)		Notes
				At 1st crack	At failure	
1 (28 days)	Internal Centre	40.0	417.0	-0.90	-5.8	Cracks visible on surface of slab at failure. Punching shear failure mode
2 (48 days)	300 mm from Edge	177.0	369.0	-4.0	-20.5	Vertical cracks followed by circumferential cracks with punching and bending failure

Table 4 (b): Summary of FEA results for slab tests 1 and 2

Test No	Slab location	Load at 1st crack, (kN)	Load at failure, (kN)	Average displacement (mm)		Notes
				At 1st crack	At failure	
1 (28 days, fck))	Internal Centre	134.0	422.0	-1.45	-5.20	Punching shear failure mode
2 (48 days, fck)	300 mm from Edge	115.0	353.0	-2.32	-16.0	Punching shear and bending failure

Table 5: Experimental results from Table 4 versus FEA results and theoretical values obtained using TR34, 4th Ed, 2018

	Theoretical (TR34, 4thEd, 2018)			Experimental			FEA		
	BM (kNm)	Punching (kN)		BM (kNm)	Punching (kN)		BM (kNm)	Punching (kN)	
Location		Face	At 2d		Face	At 2d		Face	At 2d
Centre (internal) loading No 1 (28 days)	604.50	204.17	85.90	--	417.0	--	1266	422	217
Edge Loading No 2 (300 mm) (48 days)	188.13	--	80.48	--	369.0	--	415	353	172
Corner loading No 3 (300 mm) (48 days)	34.50	--	57.61	--	--	--	112	326	154
Edge loading No 4 (150 mm)	188.13	--	63.12	--	--	--	384	220	95
Corner loading No 5 (150 mm)	34.50	--	40.25	--	--	--	103	206	91

Face = Face of contact area.
At 2d = critical control perimeter

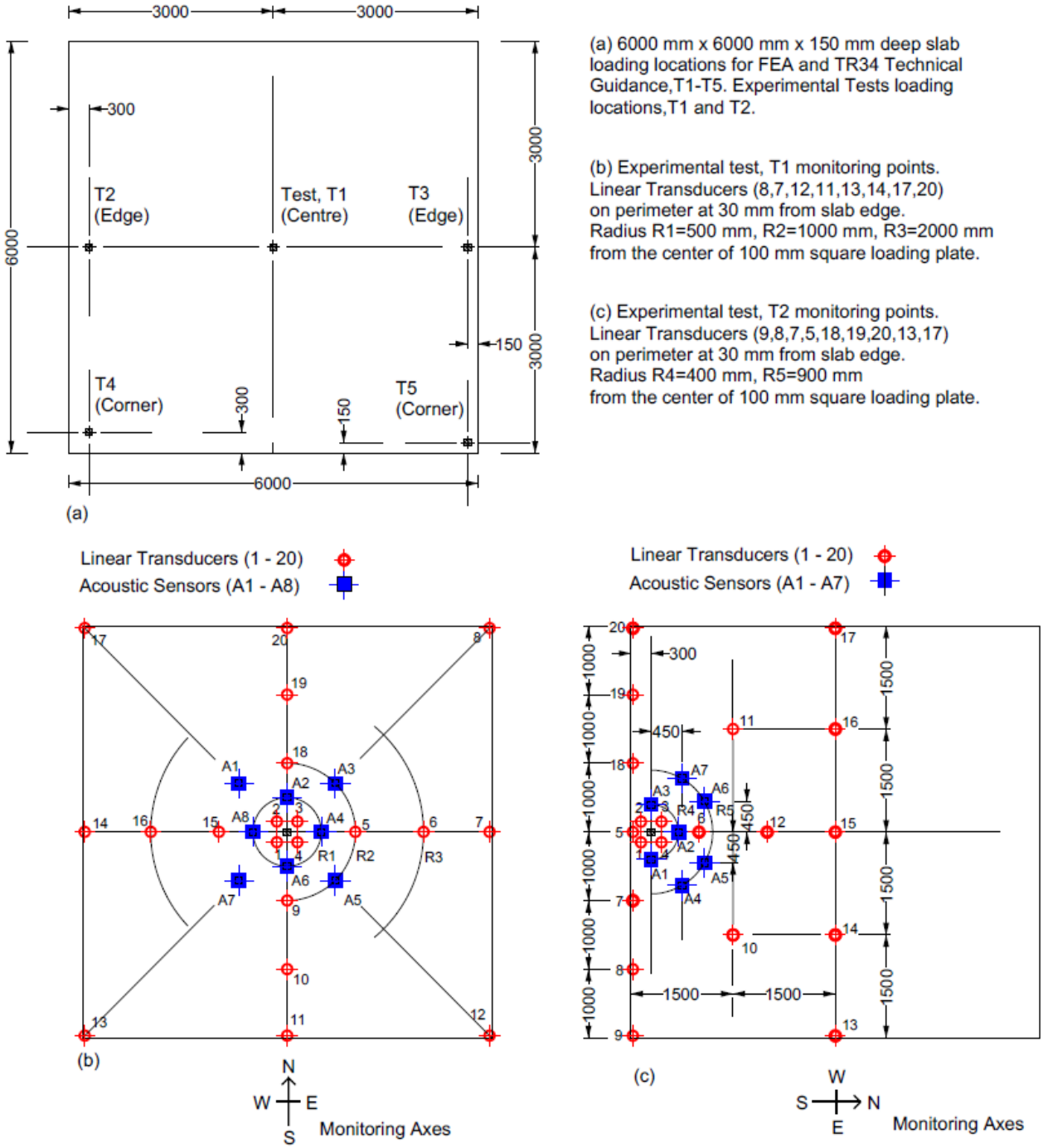

Figure 1 (a) to (c): (a) Slab loading locations for FEA and TR34 structural behaviour predictions, (b) and (c) experimental Tests monitoring locations.

(a)

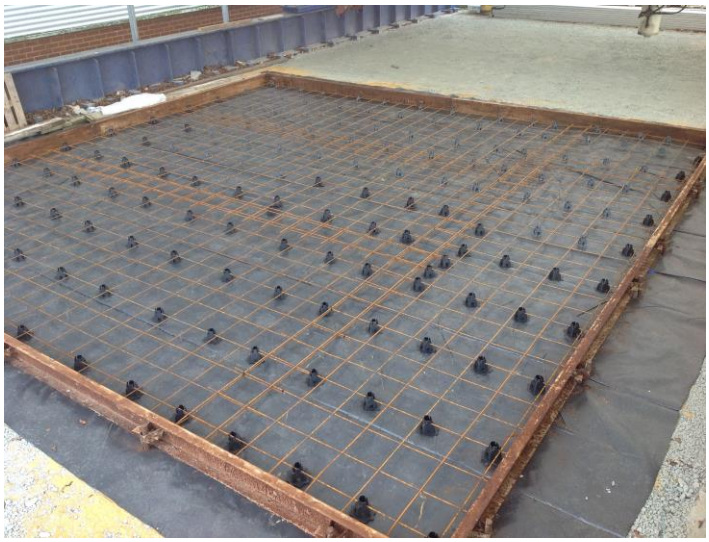

(b)

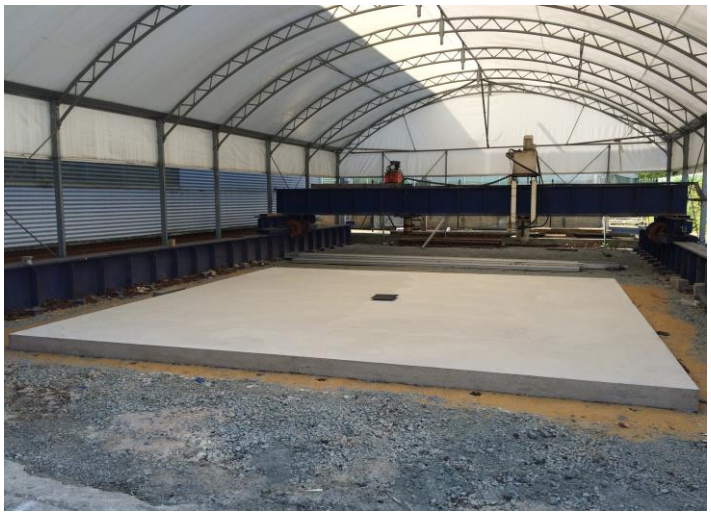

(c)

Figure 2 (a), (b) and (c): (a) Slab experimental test facilities, (b) 6 m x 6 m slab steel mesh reinforcement, and (c) cast reinforced concrete slab ready for testing.

Figure 3: 6 m x 6 m steel mesh reinforcement slab experimental Test 1 centre position viewed from the corner. Acoustic sensors, LVDTs, hydraulic jack and reaction beam visible.

Figure 4: Slab centre loading visible punching shear failure together with crack pattern.

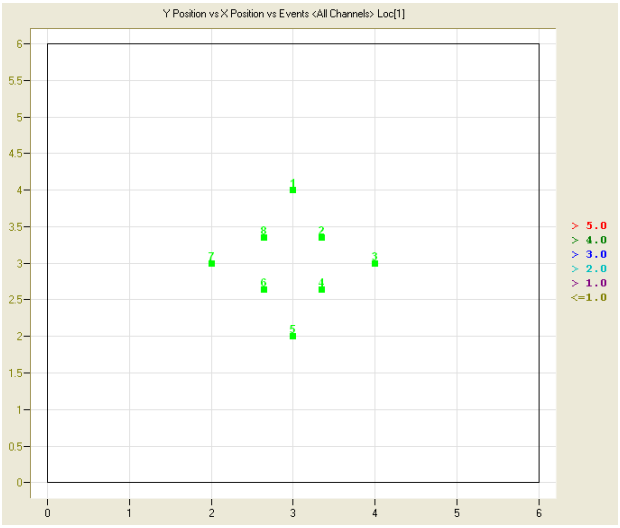

(a)

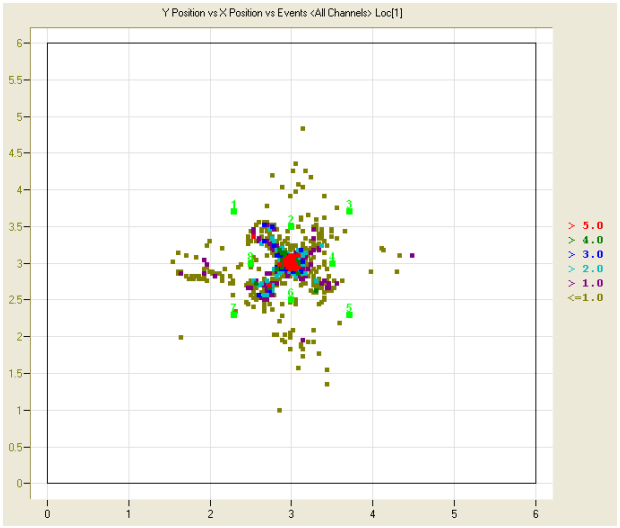

(b)

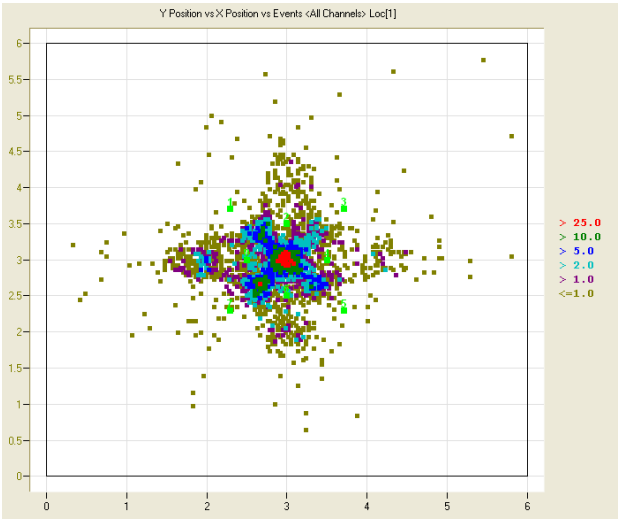

(c)

Figure 5 (a) to (c): Slab experimental Test 1 at centre crack propagation profiles in load increments to failure (a) acoustic sensors locations, (b) profile at 300 kN and (c) failure at 417 kN.

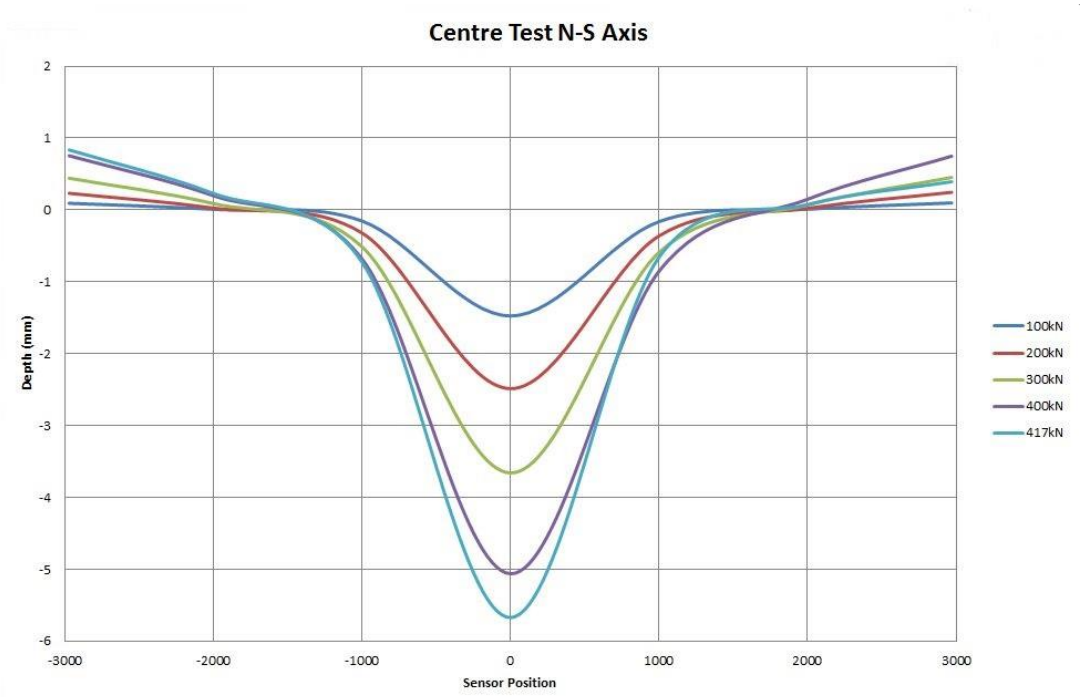

Figure 6: Slab experimental Test 1 at centre load against displacement along the 6 m monitored N-S axis caused by incremental step loading to peak failure at 417 kN.

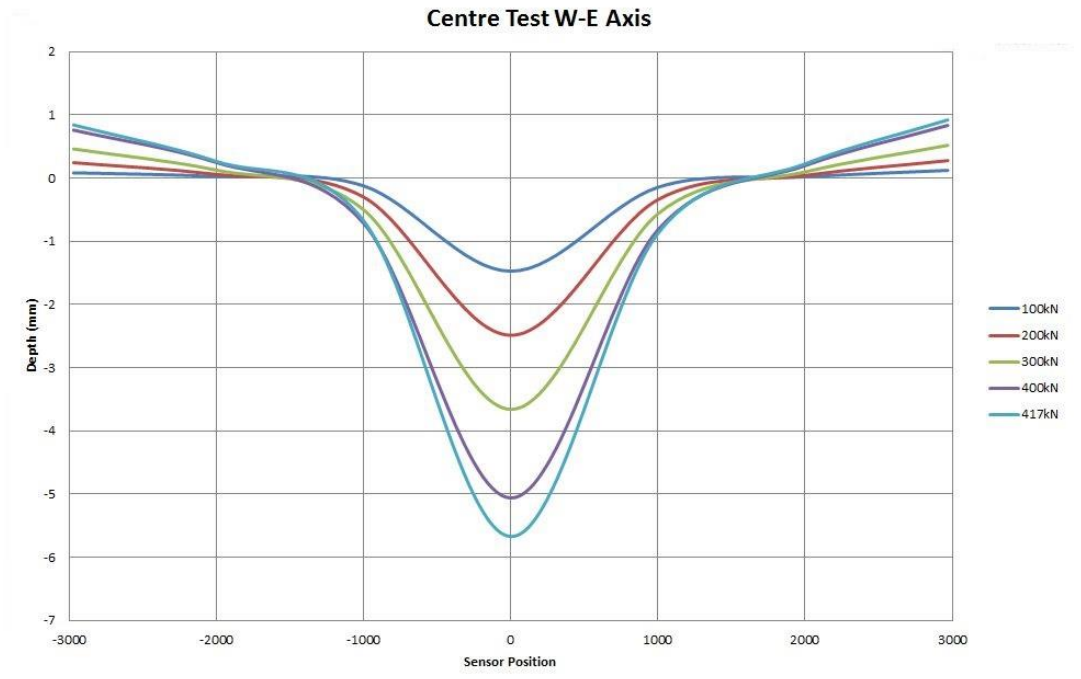

Figure 7: Slab experimental Test 1 at centre load against displacement along the 6 m monitored W-E axis caused by incremental step loading to peak failure at 417 kN.

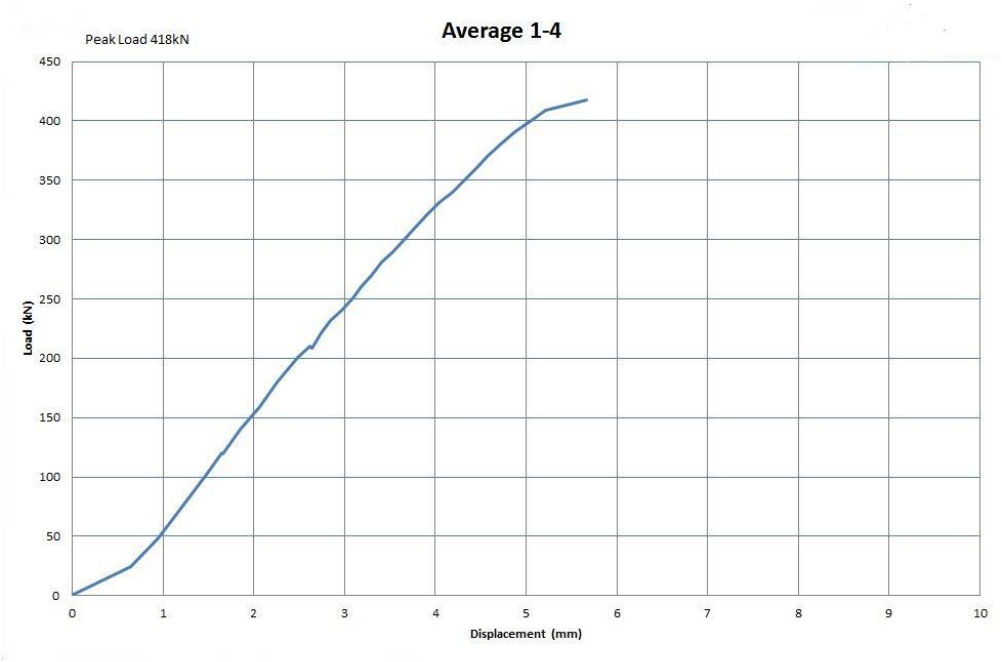

Figure 8: Slab experimental Test 1 at centre load against averaged LVDTs 1 to 4 displacements caused by incremental step loading to peak failure at 417 kN. See Figure 1 for LVDT positions.

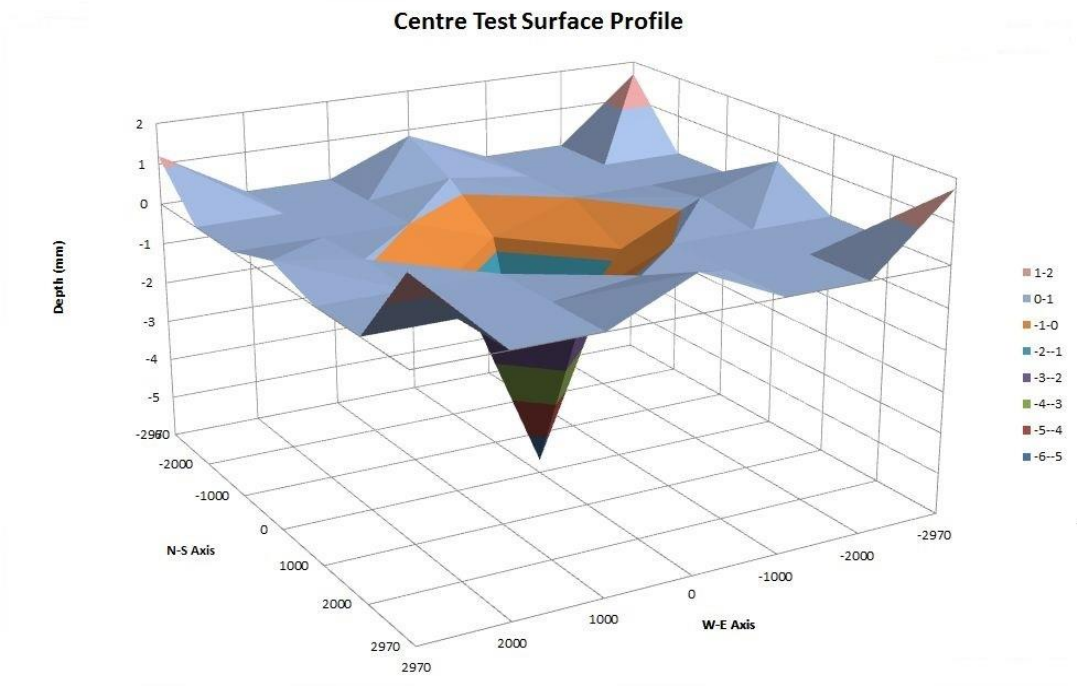

Figure 9: Slab experimental Test 1 at centre surface deformation profile due to load increments to peak failure at 417 kN.

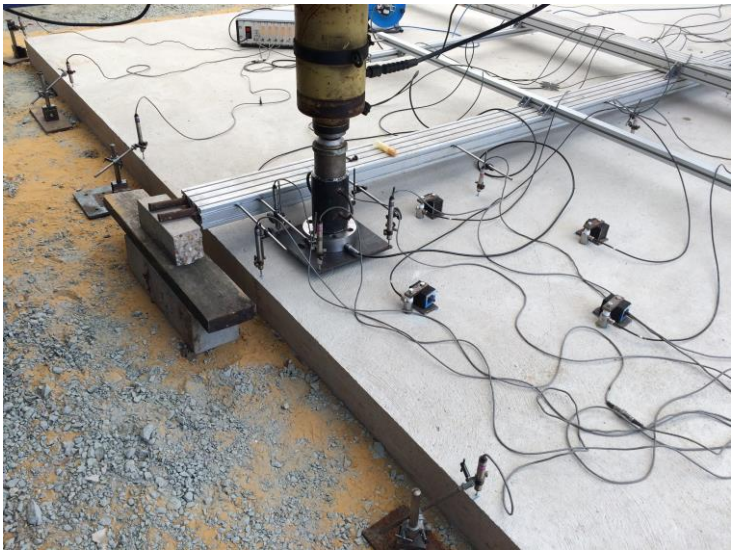

Figure 10: Experimental Test 2 Edge 300 mm position viewed from the East monitoring axes. Acoustic sensors, LVDTs, hydraulic jack and reaction beam visible.

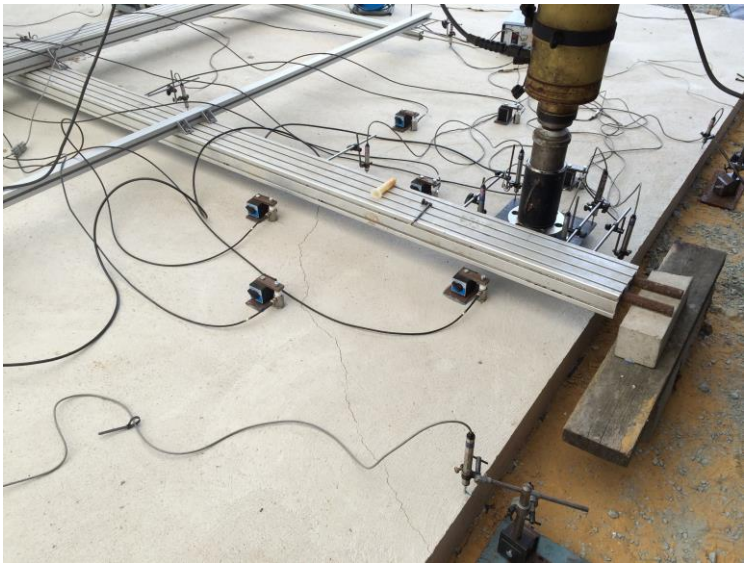

(a)

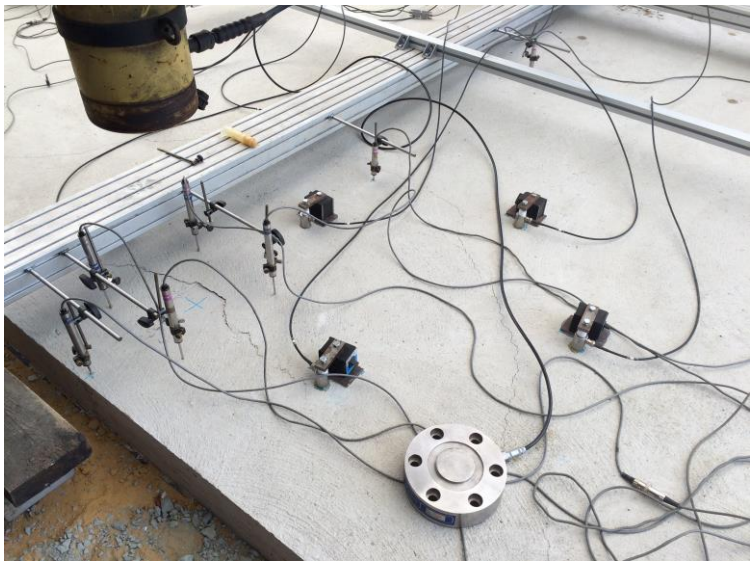

(b)

(c)

Figure 11 (a), (b) and (c): (a) Slab experimental Test 2 Edge 300 mm position visible top surface cracking viewed from the West, (b) visible top surface cracking viewed from the East, and (c) cracking visible through slab thickness.

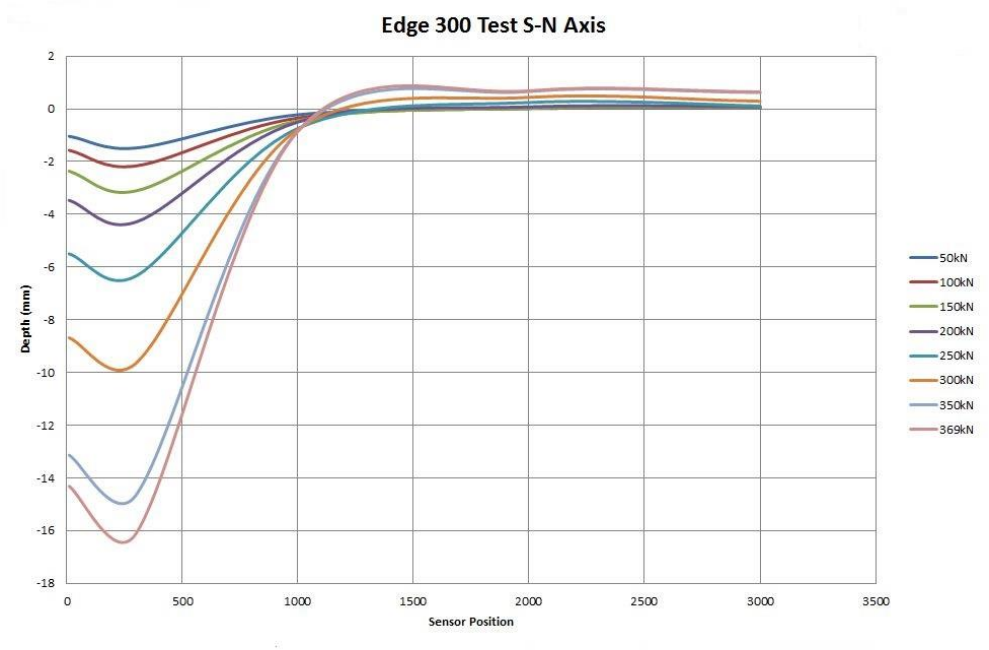

Figure 12: Slab experimental Test 2 at Edge 300 mm load against displacement along the 3 m monitored S-N axis caused by incremental step loading to peak failure at 369 kN.

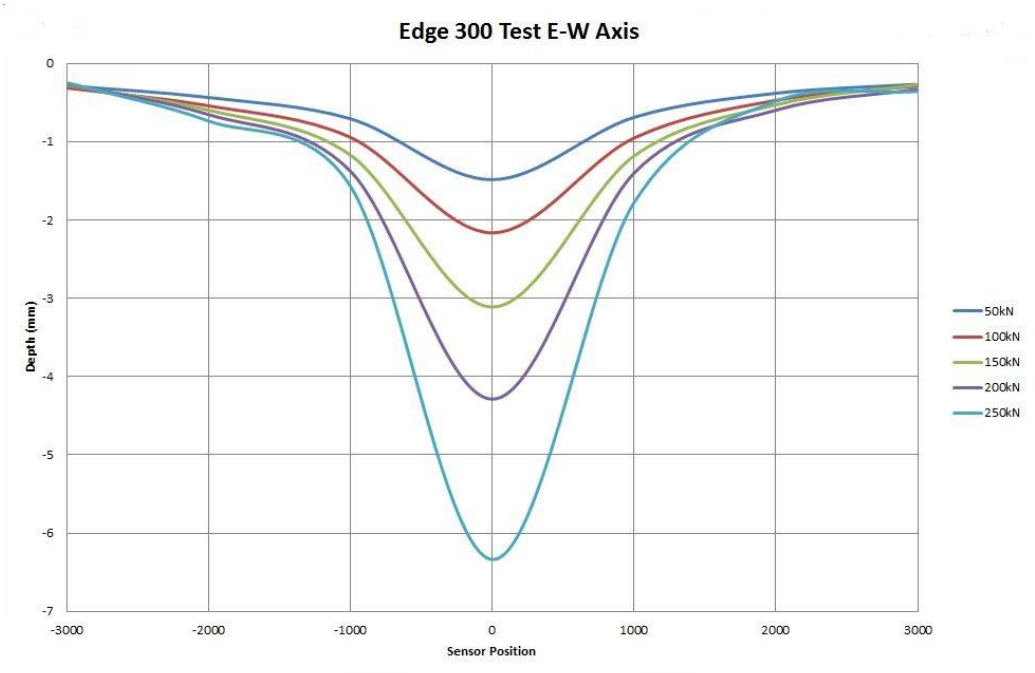

Figure 13: Slab experimental Test 2 at Edge 300 mm load against displacement along the 6 m monitored E-W axis caused by incremental step loading to peak failure at 369 kN.

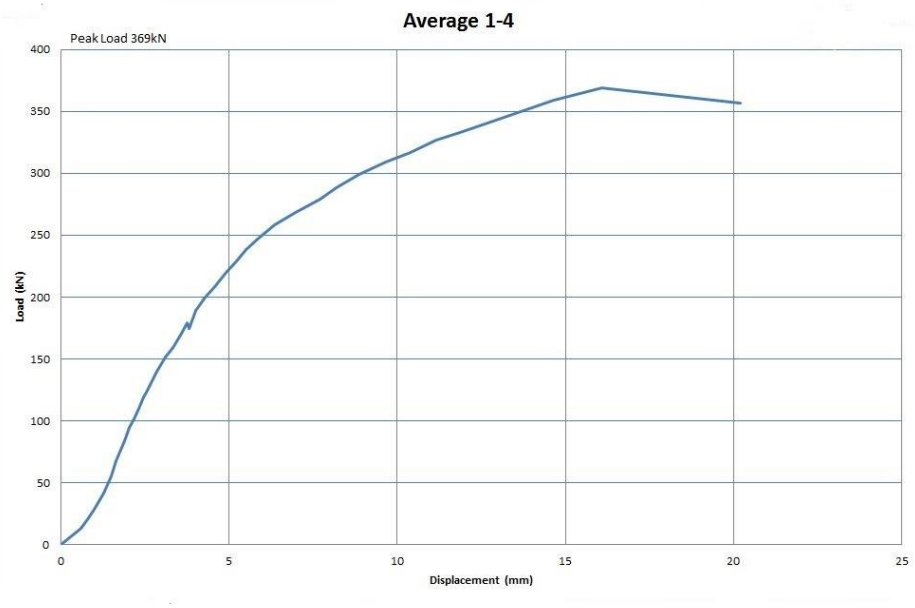

Figure 14: Slab experimental Test 2 at Edge 300 mm load against averaged LVDTs 1 to 4 displacements caused by incremental step loading to peak failure at 369 kN. See Figure 1 for LVDT positions.

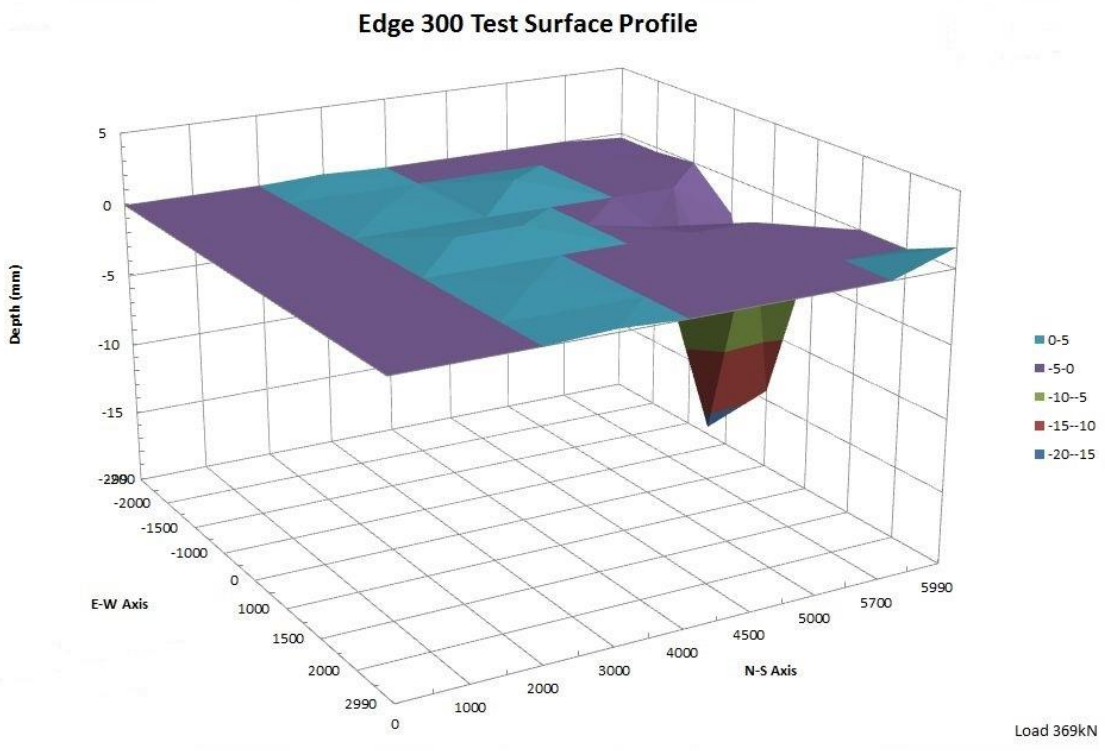

Figure 15: Slab experimental Test 2 at Edge 300 mm load surface deformation profile due to load increments to peak failure at 369 kN.

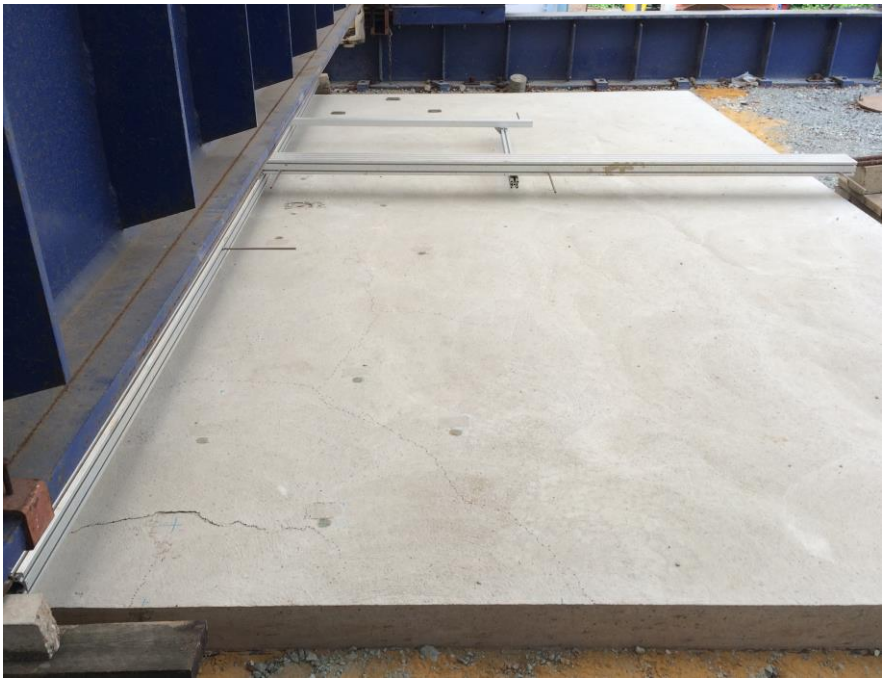

(a)

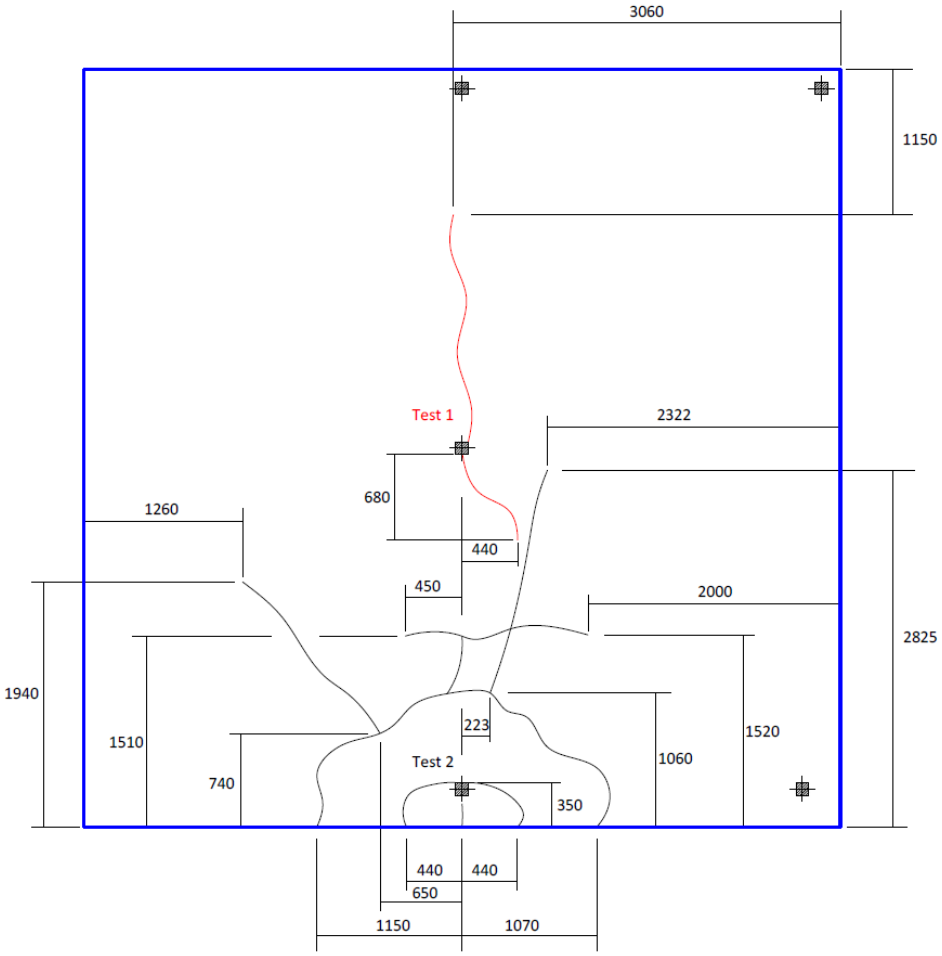

(b)

Figure 16 (a) and (b): (a) Perspective half-slab view of the experimental Test 1 at centre and Test 2 at Edge 300 mm slab top surface visible cracking patterns and (b) on plan measured visible crack patterns.

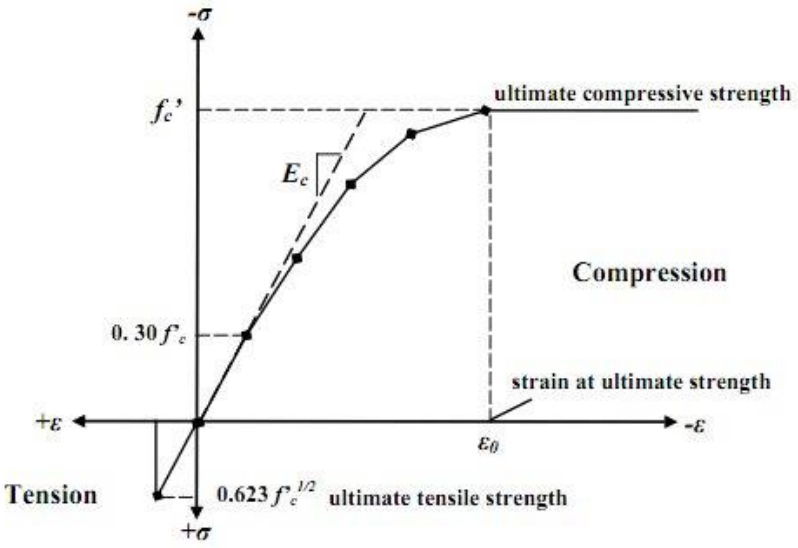

(a)

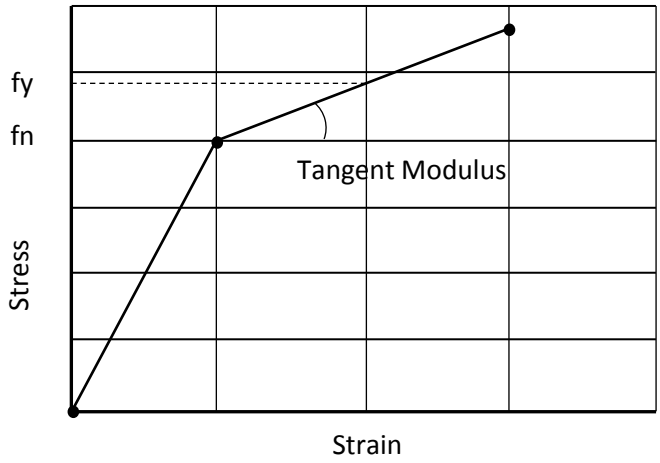

(b)

Figure 17: Idealized Stress-strain curves for the materials used in the analysis. (a) Concrete (ACI318M-19) and (b) steel reinforcement (Soroushian and Lee, 1989).

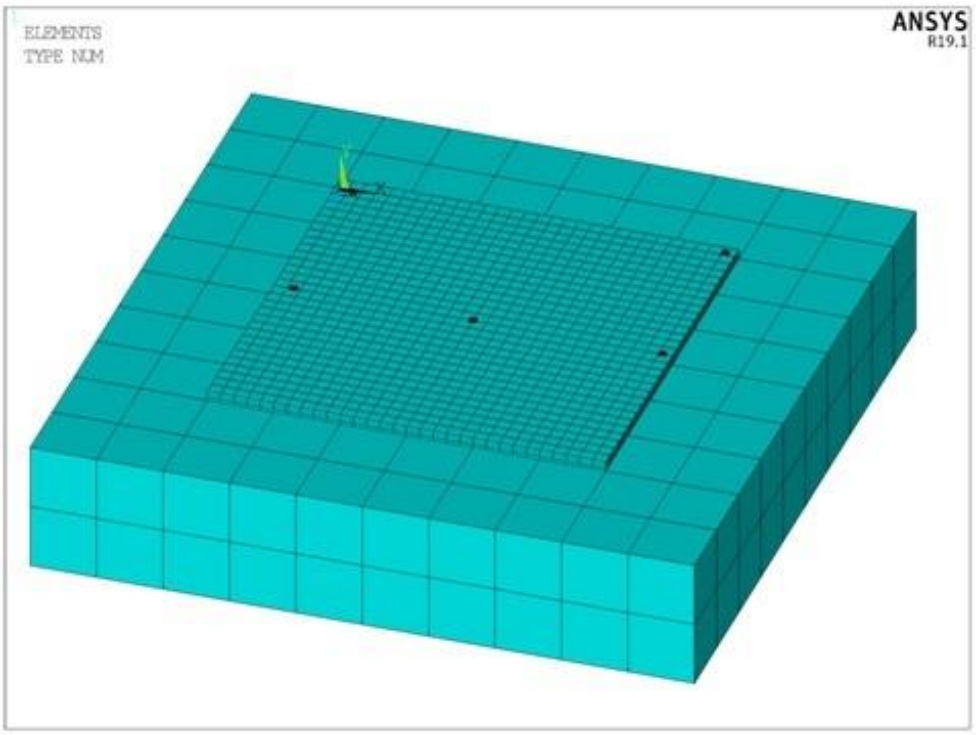

Figure 18: Typical FEA idealization of the steel mesh reinforced concrete slab, loading positions and supporting soil. See Figure 1 for applied load position dimensions.

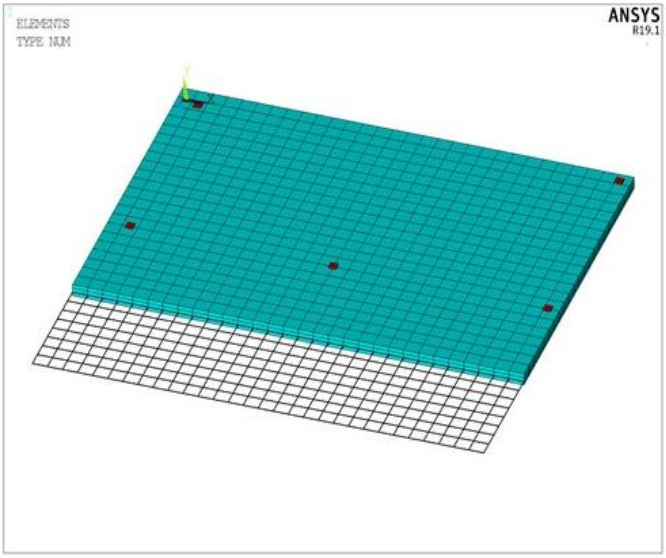

Figure 19: Detail showing 6 mm diameter at 200 mm centre to centre in both orthogonal directions steel mesh reinforcement embedded in the concrete. See Figure 1 for applied load position dimensions.

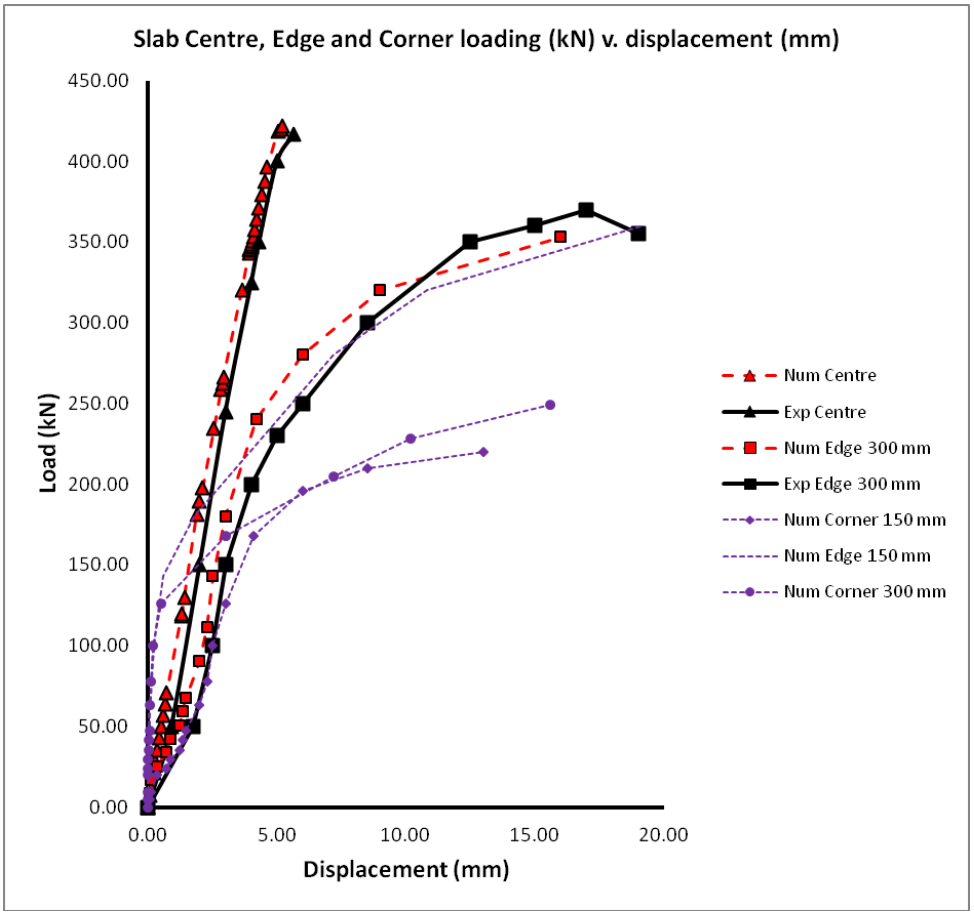

Figure 20: Experimental (Exp) and FEA (Num) load v. displacement curves for (i) centre and 300 mm edge loading, and (ii) FEA predicted curves for 150 mm edge, 300 mm corner and 150 mm corner loading.

(a) FEA Test, T1 - half slab, soffit

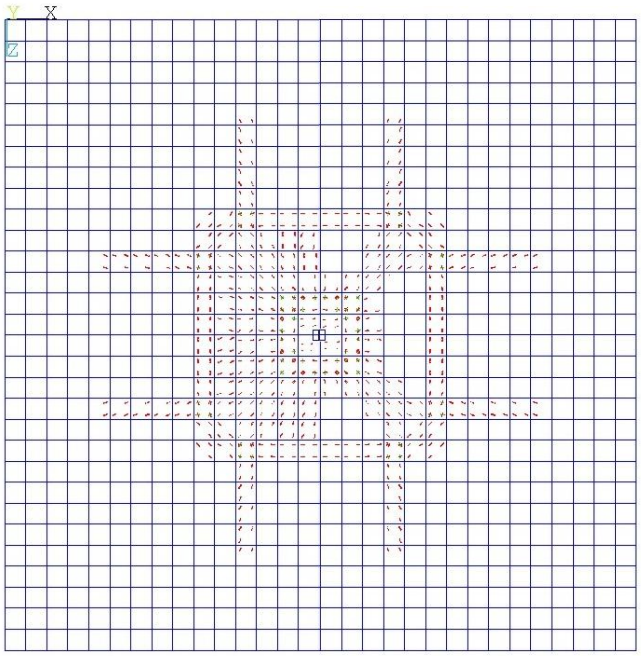

(b) FEA Test, T1 - half slab, top surface

Figure 21 (a) and (b): Slab surfaces to the left and right of centre line Test, T1 **Centre** loading. FEA centre loading predicted crack patterns (a) LHS Soffit surface, and (b) RHS top surface.

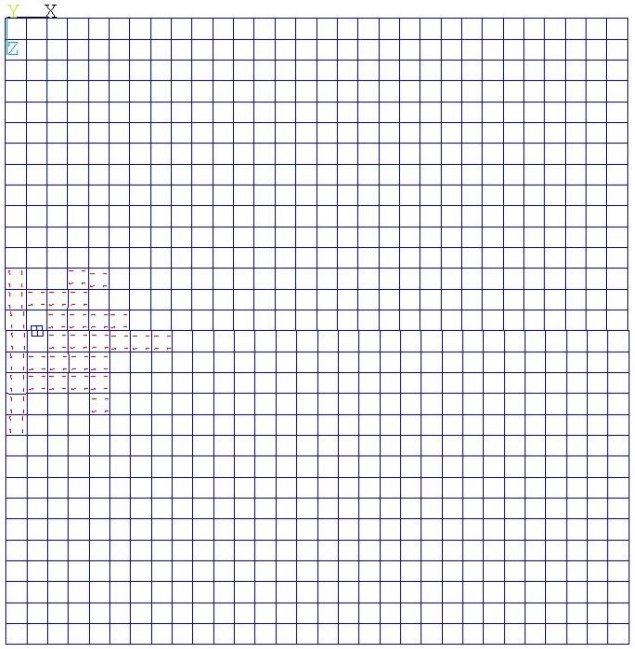

(a) Slab soffit

(b) Top surface

Figure 22 (a) and (b): Slab surfaces above and below slab centre line Test, T2 **Edge 300** mm. FEA centre loading predicted crack patterns (a) soffit surface, and (b) top surface.

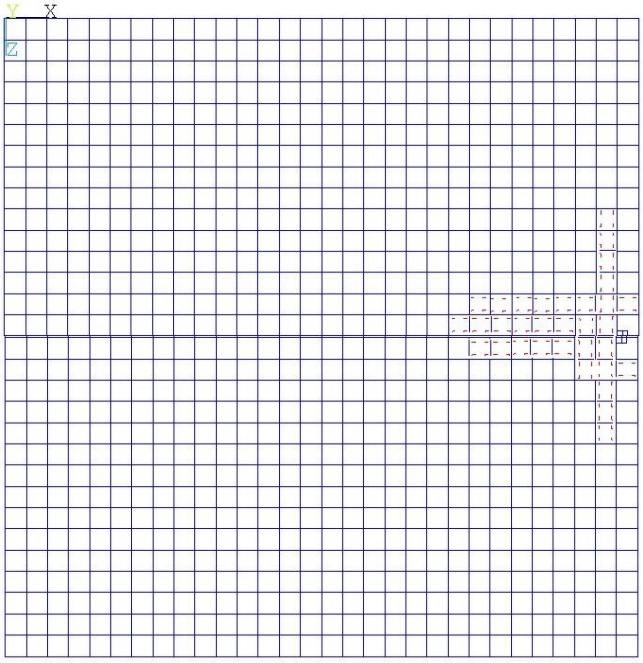

(a) Slab soffit

(b) Top surface

Figure 23 (a) and (b): Slab surfaces above and below slab centre line Test, T3 **Edge 150** mm. FEA centre loading predicted crack patterns (a) soffit surface, and (b) top surface.

(a) LHS half slab, Top surface

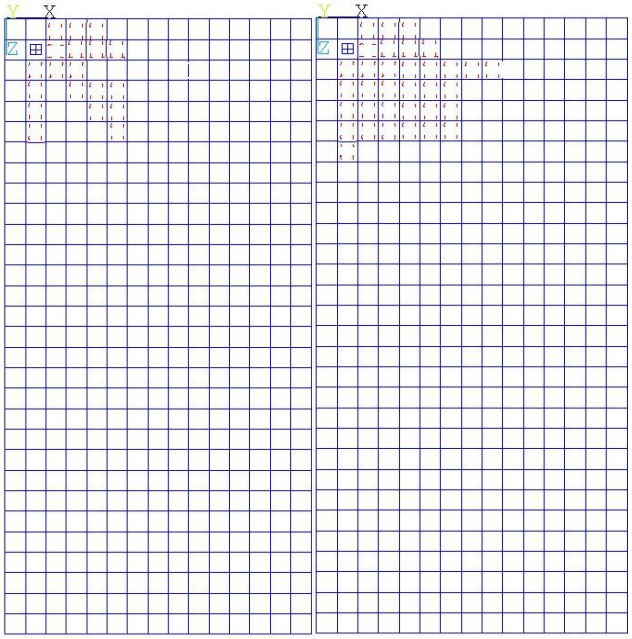

(b) LHS half slab, soffit

Figure 24 (a) and (b): Slab surfaces to the left of centre line Test, T4 **Corner 300** mm. FEA centre loading predicted crack patterns (a) LHS top surface, and (b) LHS soffit surface.

(a) RHS half slab,
Top surface

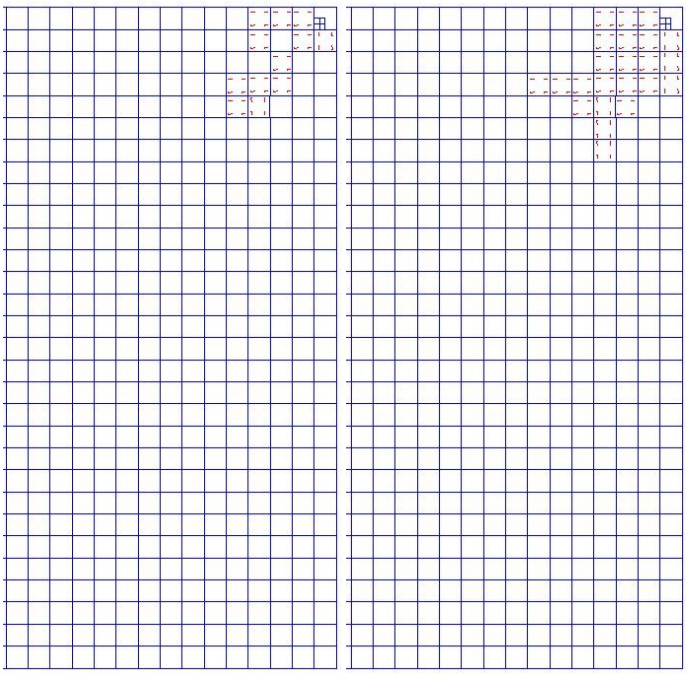

(a) RHS half slab,
soffit

Figure 25 (a) and (b): Slab surfaces to the left and right of centre line Test, T5 **Corner 150** mm. FEA centre loading predicted crack patterns (a) RHS top surface, and (b) RHS soffit surface.

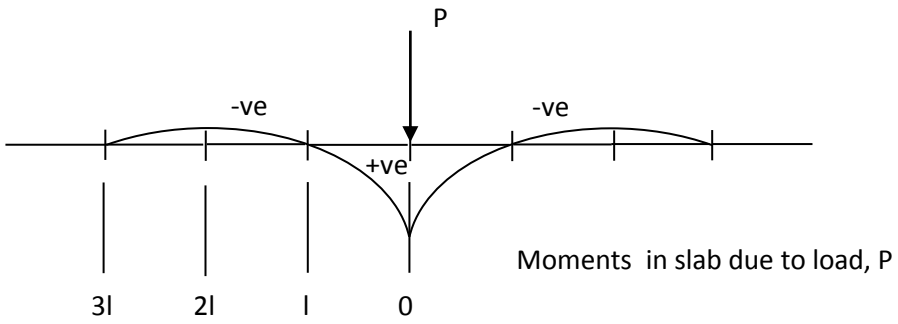

Figure 26: Schematic of distribution of elastic bending moments (TR34, 4thEd. Figure 7.1 extract)

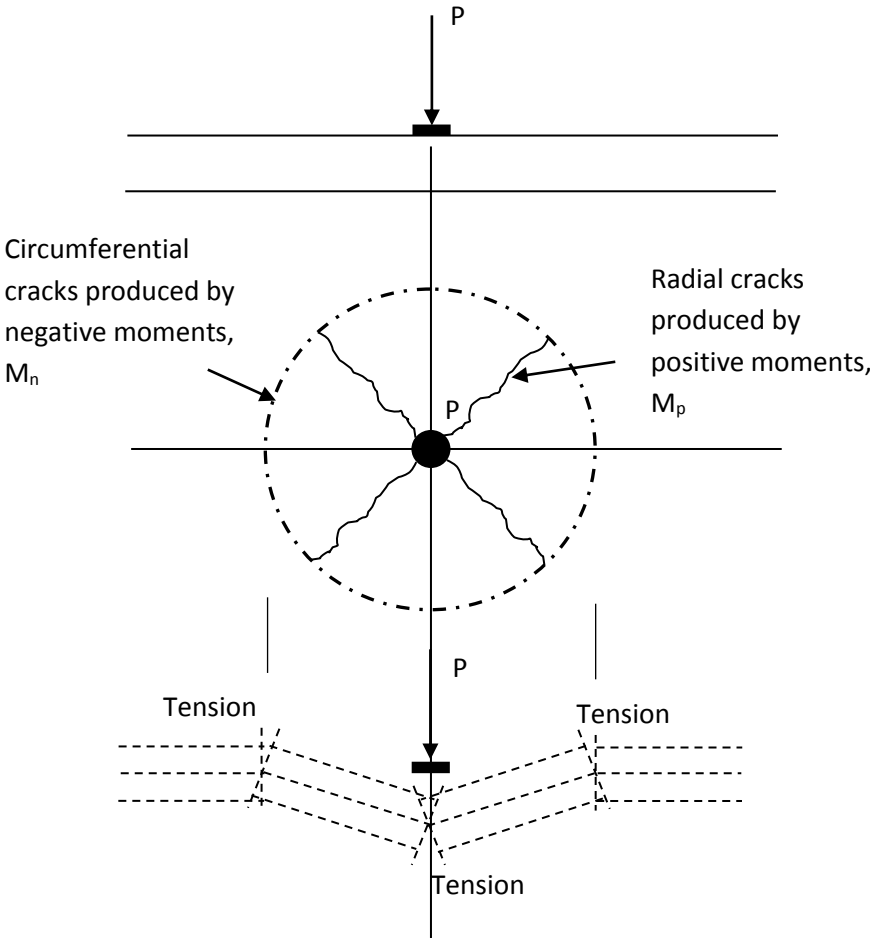

Figure 27: Development of radial and circumferential cracks in a concrete ground-supported slab (after TR34, 4thEd, Figure 7.2)

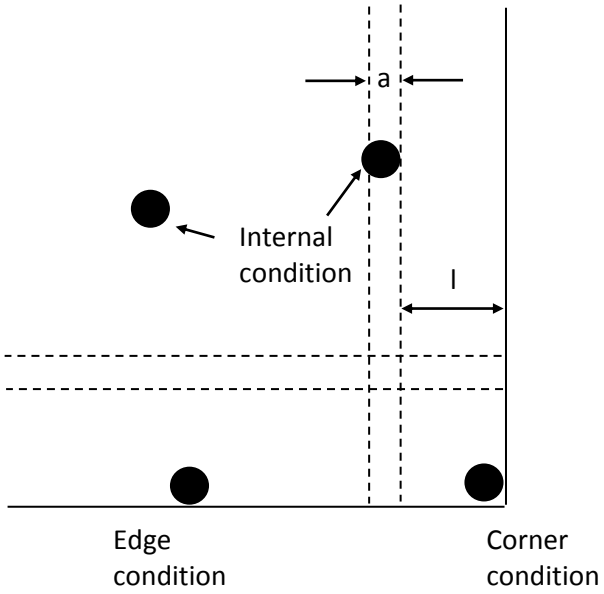

Figure 28: Definitions of loading conditions (TR34, 4thEd, Figure 7.3)

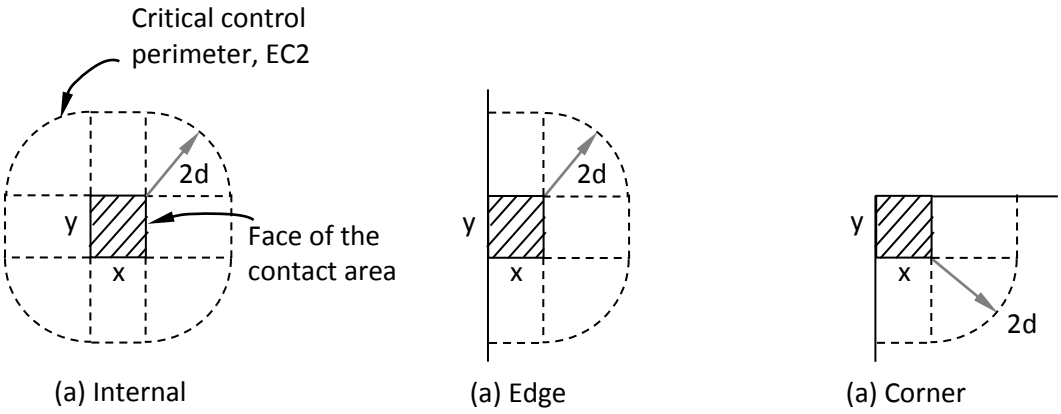

Figure 29: Critical perimeters for punching shear for internal, edge and corner loading.

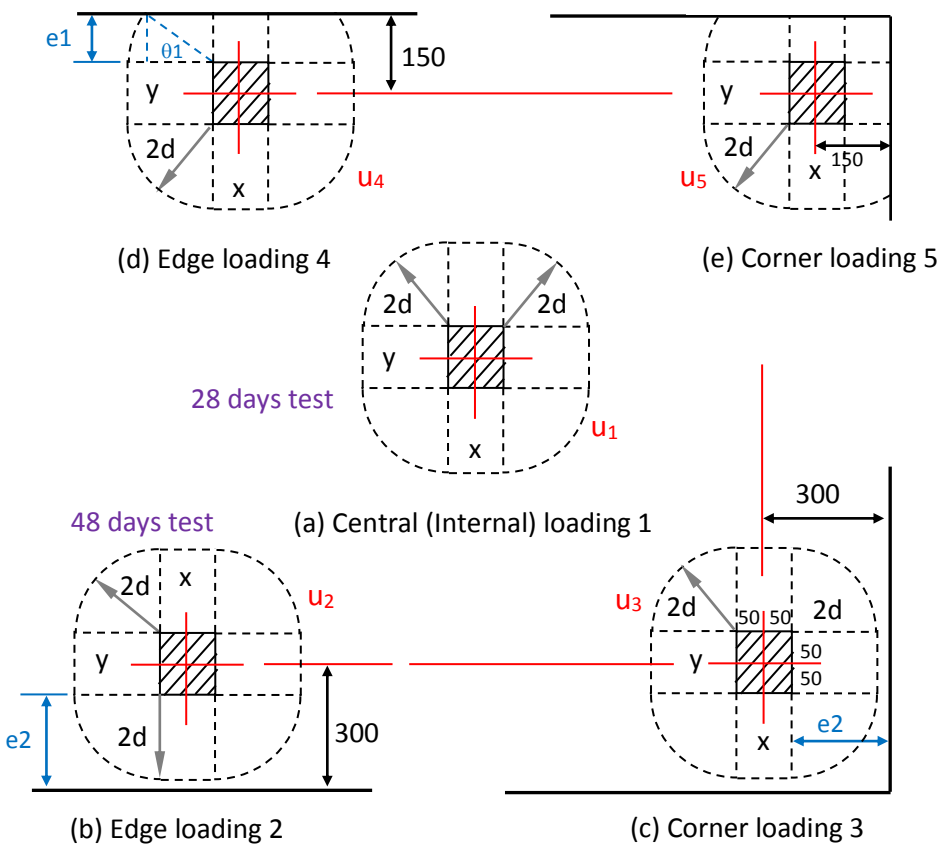

Figure 30: Experimental critical perimeters for punching shear for internal, edge and corner loading.

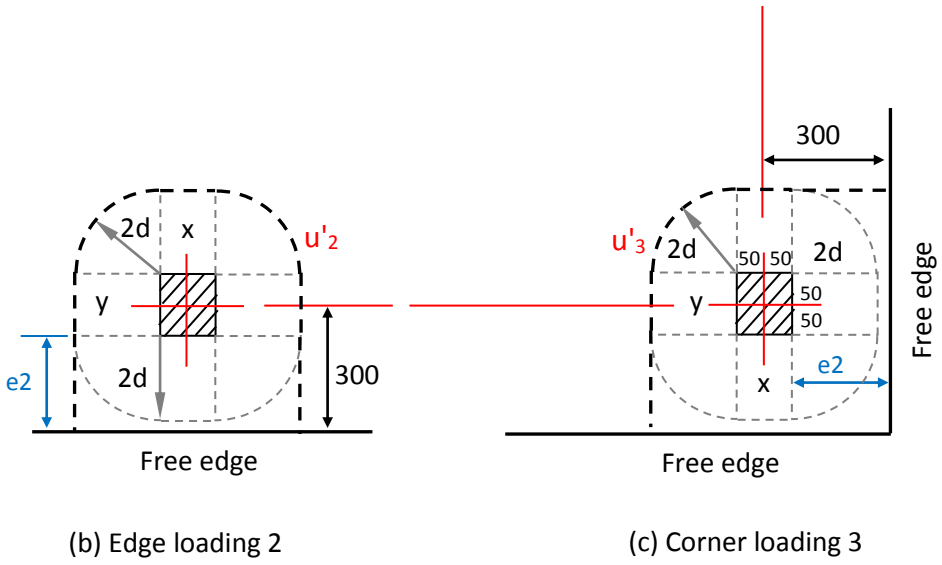

Figure 31: Minimum perimeter lengths, loading 2 and loading 3 (Loading conditions 4 and 5 similar).

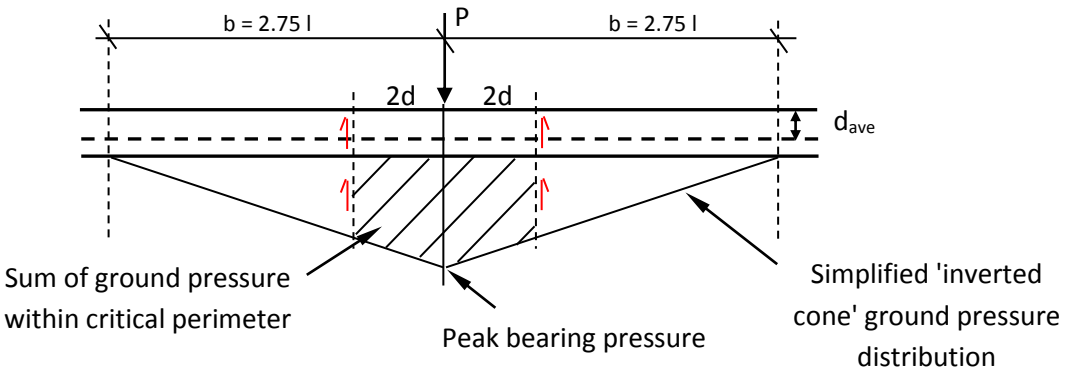

Pressure within the critical perimeter for an internal load (TR34 4th Ed, Figure F1)

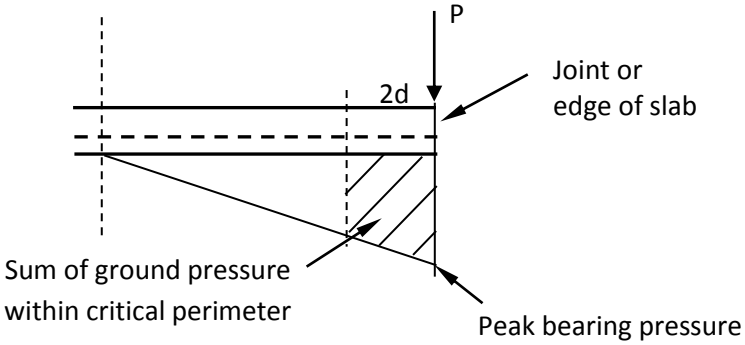

Pressure within the critical perimeter for an edge load (TR34 4th Ed, Figure F2)

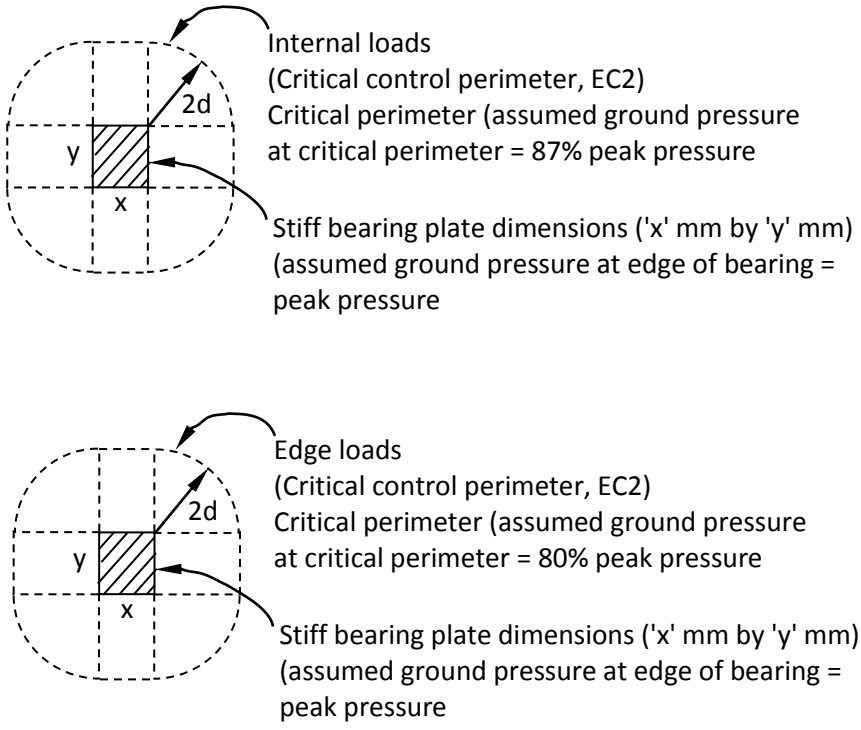

Figure 32: Pressure within the critical perimeter for an internal load and an edge load (TR34, 4th Ed, Appendix F).